EUROPEAN ORGANIZATION FOR NUCLEAR RESEARCH

NP Internal Report 71-6
18 May, 1971

LUMINOSITY AND PARTICLE DETECTION STUDIES AT THE CERN INTERSECTING STORAGE RINGS

A SURVEY MADE IN INTERSECTION #4, JANUARY - APRIL, 1971

Edited by
K.M. Potter
J.C. Sens

CONTENTS

I. INTRODUCTION

In November 1970 a working party was formed with the aim of setting up apparatus at the ISR during the running-in period of the machine in order to (as stated in the proposal CERN/ISRC/70-26):

"1) provide data on the luminosity of the ISR under various conditions of operation, of interest in the framework of performance tests on the machine itself, and

2) determine the rates and spatial distribution of secondaries resulting from beam/beam and beam/gas interactions, to the extent that such data are relevant to the design of several of the experiments which are presently under construction."

The following is a report of the activities of this working party. The measurements started on 27 January, 1971, the first day both beams were made to circulate in the ISR. Beam/beam collisions were observed almost at once; a record of the observations on that day is contained in a telex to B. Gregory, then at Brookhaven National Laboratory, U.S.A., and shown in Fig.1. The studies have been terminated at the beginning of the first ISR shut-down (7 April, 1971) and the equipment has been removed from the ISR tunnel. All measurements were made in intersection #4.

The data obtained can be divided into the two main sections mentioned above. Luminosity measurements have been done using the beam displacement technique suggested by S. v.d. Meer and, for the present time more indirectly, by measuring the profile of a single beam. Particle detection measurements have been made with a variety of instruments: scintillators, lead glass Čerenkov counters, a total absorption neutron counter, multi-wire proportional chambers, multi-element hodoscopes and emulsions, in order to identify particles and gamma rays at various angles, and to measure time of flight, dE/dX and energies of secondaries produced in beam/beam collisions. The conclusions are too numerous to be listed here - they are given at the end of each section - but in overall terms one could say that, as the ISR operating conditions improved with time, it has gradually become clear that in spite of the close proximity of the detection equipment to the circulating beams, the background conditions in the tunnel are rather more favourable than might have been anticipated. Most of the data show that with a certain number of improvements in the detection

techniques, the approved programme of experiments, for which the measurements reported here were preliminary tests, has a good chance of producing usable results. In this sense the work of this working party has been a success.

Also in another sense has the experiment been worth while. Contrary to ordinary accelerators, where physicists work in teams at the end of secondary beams, physically separated by concrete walls, the ISR demands a new style of work in which groups in a given intersection collaborate in the closest possible way in exchanging signals from different detectors, in centralizing communications, in sharing common monitors, in exchanging results of measurements, etc. The present working party comprised approximately 50 physicists, forming 8 separate teams. Much of the data reported below could not have been obtained, had each team worked in a separate intersection with its own equipment only.

It is evident that the parallel operation of running-in a new type of machine and trying to use it for physics demands a large amount of discipline both on the side of the ISR-builders and the physicists. The authors of this report would like to express their sincere appreciation for the understanding they have met in the ISR division for the problems they have been concerned with. In particular the assistance and guidance of F. Bonaudi, B. Couchman, W.C. Middelkoop and B. de Raad in preparing and carrying out the measurements and the continuous interest in our activities of K. Johnsen have been greatly appreciated.

K.M. Potter
J.C. Sens
Editors.

II. MEASUREMENT OF THE ISR LUMINOSITY

CERN/Holland/Lancaster/Manchester and CERN/British Universities Collaborations
(V. Agoritsas, B. Alper, K.M. Potter and J.C. Sens)

II.1 Method

The rate of collisions, leading to a final state of a particular kind (pp, $p n \pi^+$ etc) is given by[1]

$$R = 2 \sigma c \cos^2 \frac{\alpha}{2} \int n_1(x,y,z)\ n_2(x,y,z)\, dxdydz \qquad (1)$$

where σ is the cross section for that particular process, α the crossing angle, and $n_1(x,y,z)$ and $n_2(x,y,z)$ are the density distributions of the two beams. For equal and uniform density distributions eq.(1) reduces to

$$\bar{R}_{un} = 2 \sigma c \cos^2 \frac{\alpha}{2} \left(\frac{N_{S_1}}{2\pi R h w}\right)\left(\frac{N_{S_2}}{2\pi R h w}\right) \frac{h w^2}{\sin \alpha}$$

$$= \frac{\sigma c}{h \operatorname{tg} \frac{\alpha}{2}} \left(\frac{I_1}{e c}\right)\left(\frac{I_2}{e c}\right) \equiv L\sigma \qquad (2)$$

where R = ISR-radius, h, w = height, width of each beam
$N_{S_{1,2}}$ = number of stored protons (in ring 1 and ring 2), $I_{1,2}$ = currents ($N_S/2\pi R = I/ec$). Eq.(2) defines the luminosity as the ratio between the number of collisions leading to a particular final state and the cross section for the production of that final state. In particular, if σ is the total cross section, R is the total rate of interactions.

For arbitrary density distributions one can formally express the luminosity in terms of an effective height, h_{eff}, by equating eq.(2) to eq.(1) with $h \to h_{eff}$. It can be shown[2] that if the density distributions in the x, y and z direction are decoupled and furthermore independent of x (the coordinate in the direction of motion), h_{eff} is given by

---

1) L.W. Jones, Proc. Int. Conf. on High-Energy Accelerators, CERN 1959, p. 15.
W.C. Middelkoop and A. Schoch, CERN Report AR/Int. SG/63-40.

2) Measurement of the production of stable particles at the ISR,
A.B. Clegg et al. (CERN/Holland/Lancaster/Manchester Collaboration) CERN/ISRC/69-5, p. 24.

$$\frac{1}{h_{eff}} = \frac{\int S_1(z)\, S_2(z)\, dz}{\int S_1(z) dz \int S_2(z) dz} \tag{3}$$

where $S_1(z)$, $S_2(z)$ are the vertical density distributions of the two beams.

A method to measure h_{eff} has been suggested by v.d. Meer[3]. We repeat the principle here. One of the beams is displaced vertically with respect to the other one by an amount h. The counting rate in a monitor telescope which is sensitive to beam/beam collisions only, is equal to

$$A \int S_1(z)\ S_2(z-h)\, dz \tag{4}$$

where A is an unknown constant. By varying h over the entire region where the integrand is not zero, we can make up the quantity

$$h^* = \frac{\int [A \int S_1(z)\, S_2(z-h)\, dz]\, dh}{A \int S_1(z)\, S_2(z)\, dz}$$

$$= \frac{\int [S_1(z) \cdot \int S_2(z-h)\, dh]\, dz}{\int S_1(z)\, S_2(z)\, dz} \tag{5}$$

Since $$\int S_2(z-h)\, dh = \int S_2(z)\, dz$$

we have

$$h^* = \frac{\int [S_1(z) \cdot \int S_2(z)\, dz]\, dz}{\int S_1(z)\ S_2(z)\, dz} = \frac{\int S_1(z) dz \int S_2(z)\, dz}{\int S_1(z)\ S_2(z)\, dz} = h_{eff} \tag{6}$$

Hence h_{eff} is equal to the area under the counting rate versus displacement curve, divided by the counting rate at zero displacement.

The displacements are made by means of four steering magnets placed symmetrically around the intersection at about one quarter betatron wavelength away from the section in the up and downstream direction in each ring.

3) S. v.d. Meer, Calibration of the effective beam height in the ISR - PO/68-31.

The undisplaced beam has a vertical betatron function which has a minimum at the crossing point, and maxima in the middle of the nearest D-section at either side of the intersection, at 13.5 m (upstream) and 17.5 m (downstream) from the crossing point, see Fig. 2a. Keil and Strolin[4] have calculated the shape of the closed orbit distortion, produced by the steering magnets, Fig. 2b. This displacement has again a peak in each of the two D-sections. By adding the betatron function to the closed orbit distortion, we thus obtain that the resulting amplitude grows fastest in the D-sections and will begin to produce beam/wall background while there is still ample clearance in the crossing point, see Fig. 2c. As will be shown below this limits the range of displacements one can make in practice to about ±4 mm per beam.

II.2 Measurements

The measurements were performed with 4 scintillator telescopes. The layout is indicated in Fig. 3 and similar to an arrangement previously tested at the PS[5]. Each telescope consists of three scintillators closely surrounding the elliptical vacuum pipe. Telescope U_1 consists of the "up" counters on ring I, D_1 indicates the "down" counters on ring I, etc. In coincidences between telescopes, the one on ring I is indicated first, e.g. UD = $U_1 D_2$, etc.

Two luminosity measurements have been performed: one with 22.5/22.5 GeV beams (22/2/1971) the other with 15.3/15.3 GeV beams (5/4/1971). Some earlier data at 15.3/15.3 GeV were incomplete and will be disregarded here.

II.2.1 Small Angle Telescope Data at 22.5 GeV

A detailed discription of the various steps in the measurements of 22/2/71, at 22.5 GeV is given in the ISR Running-in report of 26/2/71. The main feature to be retained is that the beam in ring I was originally a stack of 2.03 A but, partly on purpose and partly accidentally, was scraped down to 1.28 A at the start of the measurement in I4. Beam II was 71 mA, circulating on the injection orbit. The beams were moved up and down, with always $z_1 = -z_2$.

---

4) E. Keil and P. Strolin, CERN/ISR-TH/70-8.

5) V. Agoritsas et al., CERN/71-1.

The results are shown in Figs. 4 and 5. Fig. 4 shows the combination (U_1 OR D_1) AND (U_2 OR D_2), i.e. all events with at least one particle going at small angles along each downstream pipe. The rate of accidentals was less than 0.1%. From the rate at the tails it is seen that less than 1% of the rate is due to beam/gas events. After the points at $z_1 - z_2 = 4$ and $= 8$ mm had been measured, beam I was accidentally scraped down to 0.71 A. The luminosity was not noticeably affected by this scraping, as evidenced by the symmetry of the curve and the fact that, per Amp^2, the rate at 0 displacement remained unaltered. Between $|z| = 4$ and $|z| = 6$ mm in either beam the background increases sharply, indicating the onset of beam/wall interactions in the regions of large betatron amplitude, as discussed above. At $z_1 = +6$ and $z_2 = -6$ mm the accidental/real coincidence ratio is 100%.

The effective height is obtained by dividing the area under the curve in Fig. 4 by the height at 0 displacement:

$$h_{eff} = 5.1 \text{ mm}$$

with an error of perhaps a few percent (too few points have been measured to quote a meaningful error). The luminosity is then:

$$L = \frac{1}{e^2 \, c \, h_{eff} \, tg \frac{\alpha}{2}} = 2.0 \times 10^{28} / cm^2 / sec / A / A$$

Fig. 5 shows the counting rates in the combinations UD, DU, UU and DD. The beam/gas rate is less than $\sim$ 3% for all combinations. The UD and DU rates correspond to elastic + inelastic beam/beam events, while the UU and DD rates correspond to inelastic beam/beam events only. A timing error in the D_1 telescope, found after the data had been taken, affected the efficiency of the combinations DU and DD, and hence no comparison of the four peak rates can be made. This error had been corrected before further luminosity measurements were made. The effective heights obtained from the UU and UD data are in good agreement with the "OR" data of Fig. 4 (UU: h = 4.9 mm; UD: 5.0 mm).

From the luminosity measured above and an assumed value for the cross section σ, we can estimate the efficiency η of the monitor for counting colliding beam events from the relation

$$R_M = \eta R = \eta L \sigma$$

where R is the rate of colliding beam events and R_M is the rate in the monitor. For (U_1 OR D_1) AND (U_2 OR D_2), UU and UD we find respectively:

$$\eta_{OR} = 4.8\ \% \qquad \eta_{UU} = 1.25\% \qquad \eta_{UD} = 1.8\%$$

if we assume σ = 40 mb.

II.2.2 Small Angle Telescope Data at 15.3 GeV

Fig. 6 shows the data taken with 15.3/15.3 GeV beams, for the combinations UU, DD, UD and DU (no (U_1 OR D_1) AND (U_2 OR D_2) data were taken during this run). During this measurement strong beam/wall effects were present in both beams, resulting in accidental/real ratios ranging between ~ 10% and ~ 75% in all combinations. The effect of beam/wall interactions on the rates in the single telescopes U_1, D_1, U_2 and D_2 is illustrated in Figs. 7 and 8. Fig. 7 shows an increase by two orders of magnitude in the rates in U_1 and D_1 for a 3 mm downwards displacement of beam I. Fig. 8 shows that a displacement of at least + 2 mm is required to eliminate beam/wall interactions as the main source of particles in U_2 and D_2. From Figs. 7 and 8 it may be anticipated that for displacements $z_1 - z_2$, for which $z_1 > 0$ and $z_2 > 2$ mm, the combinations UU etc. will have low accidental rates. This is borne out by data taken with z_1 = + 1.5, z_2 = + 3.5 and z_1 = + 1.5, z_2 = + 2.5 mm (closed circles in Fig. 6), for which the accidental/real ratio was < 0.3%.

The effective height at 15.3 GeV as deduced from the areas under the curves of Fig. 6 are:

UU : h = 5.1 mm UD : h = 5.3 mm

DD : h = 5.0 mm DU : h = 5.4 mm .

From the peak rates in Fig. 6 one obtains for the efficiencies η

η_{UU} = 0.45% η_{UD} = 0.95%

η_{DD} = 0.34% η_{DU} = 0.90%

for $L = 2.0 \times 10^{28}/cm^2/sec/A^2$ and σ = 40 mb.

II.2.3 Miscellaneous Observations

A potential source of error is the variation of $\Delta\Omega$ with the z-coordinate of the point of interaction.

The agreement between the effective heights obtained from the UU and DD data with those from the UD and DU data indicates that this dependence is weak. Furthermore, by comparing the data for $z_1 - z_2 = -1$ mm with the centre line of the intersecting diamond at $z = 0$ and at $z = +2$ mm one obtains within errors the same rates in all combinations UU, DD, UD and DU. This indicates that the dependence of $\Delta\Omega$ on z can be neglected, at least until more detailed measurements have been made.

Data have also been taken in order to establish whether or not steering the beams vertically in one intersection would influence the rates in another. Fig. 9 shows data obtained at 22.5/22.5 GeV in the course of the luminosity measurements in intersection I5. Similar results were obtained in the 15.3/15.3 GeV run. It is seen that the closed orbit distortion centred on I5 has no detectable effect on the rates in I4, at least as long as the beams remain clear of the walls. Hence luminosity measurements can be done in a given intersection while data taking can continue in the others.

Some data were also obtained on the variation of effective height, or luminosity per unit currents, with time. With the rings set at working point "FATA FS15" Fig. 10 shows a ~ 10% increase in effective height over an $8^1/_2$ hour period, in which the beams were left circulating without any adjustments. At the same time, a gradual reduction in the number of beam/wall interactions was observed.

The counting rates in the individual scintillators surrounding the downstream pipes (see Fig. 3) have been measured in quiet conditions with ~ 700 mA in each ring, and with the beams dumped. The difference averaged over 12 scintillators (40 cm wide, 20 cm high, with semi-elliptical cut-out) is ~ 850/sec/Amp, i.e. about 1 particle/sec/Amp/cm^2.

By placing a liquid Čerenkov counter (FC 75; effective threshold $\beta \approx 0.8$) behind one of the small angle telescopes it was established that at least 85% of the particles in the downstream hodoscopes have $\beta > 0.8$. Correcting a difference in solid angle would take this number closer to 100%.

Finally, time of flight data were obtained between the telescopes on opposite downstream arms. One expects in principle to see three peaks: one originating from beam/beam collisions in the intersection, and two others from straight-through particles (in the downstream directions of ring I and II, respectively). Since the counters were designed to have as little overlap as possible for particles travelling outside and parallel to either of the pipes, the two latter peaks are not observed in the time-of-flight spectrum, See Fig. 11.

Luminosity data taken with a total absorption counter, set to count both charged and neutral particles, in coincidence with one arm of the small angle telescopes will be reported in section V; data taken with a multi-counter set-up will be reported in section XI.

II.3 Comparison between Measured and Expected Rates of Events

II.3.1 Inelastic Beam/Beam Events

We define inelastic events as beam/beam collisions resulting in at least one secondary entering one telescope in coincidence with another secondary passing through another non colinear telescope. We assume that the multiplicity is so large that by removing one particle the distribution of the remaining ones remains unaltered. The rate of inelastic events in a single telescope is then given by

$$N_S = L \sigma M \Delta\Omega \quad \text{sec}^{-1}$$

where $L = 2.0 \times 10^{28}$ cm^{-2} sec^{-1}

$\sigma = 40$ mb

M = number of secondaries/sr/interacting proton (from thermodynamical model)

$\Delta\Omega$ = solid angle of one telescope.

The rate of inelastic events in two telescopes subtending the same angular range, with the same solid angle is given by

$$N_D = L \sigma (M \, d\Omega)^2 \quad \text{sec}^{-1}$$

Each of the four telescopes subtends the angular range Θ = 6.5 - 25 mrad. The counters have semi-elliptical cut-outs (see Fig. 3), and hence the solid angle depends on Θ. From the values of $M \Delta \Omega$, obtained from the thermodynamical model and integrated over the angular range we find for the expected contribution of inelastic events to the rates in the single and double telescopes:

	15 GeV	22 GeV	
N_S	74	138	particles/sec/Amp/Amp
N_D	7	24	

while experimentally we have, for the average of the UU and DD rates:

N_D(exp)	3.2 ± 0.2	9.6 ± 0.3	particles/sec/Amp/Amp

Hence the observed rates are a factor ~ 2.5 lower than predicted, while for the scaling from 15 to 22 GeV there is agreement.

II.3.2 Beam/Gas Events

The dominant source of particles in the single telescopes are beam/gas events. In order to estimate this contribution we assume that the telescopes see beam/gas events produced over a length of ~ 10 m. This gives, for ~ 100 secondaries/ beam/gas collision/sr (at 15 GeV, from thermodynamical model) and $\Delta\Omega \approx 9 \times 10^{-4}$ sr, N_S(beam/gas) = 60/sec/Amp. Comparing with observed single telescope rates we then have:

N_S (beam/gas + inelastic beam/beam)	≈	130/sec/Amp
N_S (exp.)	≈	250/sec/Amp

where the measured rate is an average of the rates in the most quiet conditions (corresponding to vertically displaced beams, see above) in ring I and ring II at 15 GeV.

II.3.3 Elastic Beam/Beam Events

At the peak of the luminosity curves the count rates in the four combinations are :

	UU	DD	UD	DU	
15 GeV	3.6	2.7	7.5	7.2	particles/sec/Amp/Amp
22 "	10	~10	15	~15	" " " "

(the 22 GeV DD and DU data were scaled from data taken during a different run). One thus expects the contribution of elastic events to be of the order of 4 events/sec/Amp/Amp both at 15 and 22 GeV. In order to check this we have calculated the elastic rate, under the following assumptions:

15 GeV σ_{el} = 5.0 mb b = 12.2 GeV^{-2} L = $2.0 \times 10^{28}/cm^2/sec/Amp/Amp$

22 GeV σ_{el} = 5.0 mb b = 15 GeV^{-2} L = $2.0 \times 10^{28}/cm^2/sec/Amp/Amp$.

with the result

15 GeV N_{el} = 33 events/sec/Amp/Amp

22 GeV N_{el} = 27 events/sec/Amp/Amp

i.e. a factor ~ 8 higher than is observed. We have no quantitative explanation for this disagreement. It may be noted only that, for the angular range accepted by the telescopes, the effective thickness of the vacuum pipe ranges from 93 to 350 mm, i.e. from ~ 1 to 3 collision lengths. This underlines the fact that without thin walls, transitions, cones, etc. no accurate measurements at small angles can be made.

II.4 Conclusions

1) Scintillator telescopes placed at small angles along the downstream pipes are adequate to measure the luminosity by the beam displacement technique of v.d.Meer. Within the present accuracy of about 5% no systematic effects have been detected which could affect the results.

2) The effective height is approximately 5 mm, both at 15 and 22 GeV, i.e. well within the design value of the ISR. This corresponds to a luminosity of $2 \times 10^{28}/cm^2/sec/Amp/Amp$.

3) The efficiency of the combined telescopes ((U_1 OR D_1) AND (U_2 OR D_2)) defined as the ratio between the rate and the number of collisions, assuming σ = 40 mb, is ~ 1.5% at 15 GeV and ~ 5% at 22 GeV and corresponds to ~ 20 (50) counts/sec/Amp/Amp at 15 (22) GeV.

4) The combined contributions of beam/gas events, accidentals, etc. to the rates in any of the combinations UU, DD, UD and DU are less than ~ 3%.

5) The rates in the single (threefold) telescopes (which cover the angular range 6.5 - 25 mrad, with a solid angle of ~ 0.9 msr) are in reasonable agreement with the rates calculated from the thermodynamical model, if both beam/gas and beam/beam events are taken into acccunt. The beam/gas contribution is at least 50% of the total rate. More than 85% of the particles have been measured to have $\beta > 0.8$.

6) The rates in the two-arm telescopes UU and DD are lower by a factor ~ 2.5 than expected on the basis of inelastic beam/beam events. The increase from 15 to 22 GeV is in agreement with expectation.

7) Although there is an excess of coplanar over non-coplanar events, this excess is in disagreement with the rate expected for elastic scattering with reasonable parameters. This probably results from scattering and interactions in the walls of the vacuum pipe.

8) Within limits, a luminosity measurement in one intersection need not disturb the conditions in another.

9) For at least one working point of the ISR, the effective height has been observed to vary slowly (~ 10% increase in $8^1/_2$ hours) with time.

10) Near the pipes the number of particles passing thrcugh a surface perpendicular to the pipes is approximately $1/sec/Amp/cm^2$.

III. BEAM PROFILE MEASUREMENTS

CERN/Holland/Lancaster/Manchester and British/Scandinavian/
CERN Collaborations
(V. Agoritsas, B. Alper, B. Bošnjaković, K.M. Potter, J.C. Sens)

Introduction

If the vertical profile of each ISR beam and their relative vertical positions at an intersection can be measured, it will be possible to calculate the luminosity without any need to move or otherwise disturb the beams. In addition, a suitable beam profile monitor would give a useful check on any distortion of the beam profile during beam displacements. In order to determine a beam profile, the beam's interaction with the residual gas can be used. However, the residual gas pressure close to an intersection is so low, typically 3×10^{-11} torr, that counting rates are extremely low. A measurement of the beam profile at I4 was obtained with a scintillation counter monitor, as described below, but only with a raised gas pressure.

The Beam Profile Hodoscopes

A beam profile monitor was set up three metres upstream of intersection I4 on ring 1. A schematic plan of the arrangement is shown in Fig. 12. The two identical hodoscopes H_1 and H_2 consisted of seven scintillators 5 mm by 6 mm high by 300 mm long arranged as a picket fence to give horizontal bins each 2 mm high. A scintillation counter (SC) covered the whole area of H_1 and H_2 and the counter (V) was used in anti-coincidence to reduce the effects of upstream background. A liquid Čerenkov counter (C) with a β threshold of 0.78 was used to eliminate low-energy particles. The hodoscopes H_1 and H_2 were mounted on vertical scanning tables and positioned at the same height to an accuracy of better than half a millimetre.

The logic used to obtain 13 bins from each set of overlapping scintillators is shown in Fig. 13. From the logic diagram it can be seen that each bin of H_1 was put in coincidence with the corresponding bin of H_2 and individually scaled. Two identical logic circuits, with inputs from each of the scintillators of each hodoscope, ensured that only events in which one particle traversed the hodoscopes were recorded. Thus the arrangement accepted only beam-gas secondary particles in an approximately

horizontal plane from a metre of beam at a mean scattering angle of 350 mrad.

The vertical resolution of the monitor estimated to be ± 3 mm, was almost entirely governed by the multiple scattering of the secondaries in the 2 mm thick vacuum pipe. The mean momentum of particles scattered at 350 mrad from a 25 GeV beam is approximately 1 GeV/c so that the projected scattering angle $\sqrt{\bar{\theta}_S^2}$ = 9 mrad, giving a mean vertical error at the beam of ± 2.7 mm.

The event rate with the arrangement described was calculated to be approximately 1/sec for a 20 amp beam with 10^{-10} torr of residual hydrogen .

Results

With the normal gas pressure and beams of around one amp, it was found impossible to obtain a beam profile. The very low counting rate (~ 2/ minute) was swamped by other effects due to the general background. The local gas pressure was therefore raised by heating the vacuum chamber with the normal bake-out jackets. In this way the pressure was raised to 3×10^{-9} torr as recorded by the adjacent gauges. The counting rate in each bin was then a few per second with a 600 mA, 15 GeV beam in ring 1.

The hodoscopes were designed with the intention of measuring the profile by scaling the rates in each bin, leaving the hodoscopes in a fixed position. In practice the counters were not equally efficient and hence it was decided to scan both H_1 and H_2 vertically and to scale the rates in each bin as a function of the vertical position of that bin. In this way several profiles were obtained simultaneously. The outer elements of the hodoscopes did not yield useful profiles because the total displacement was not large enough. Fig. 14 shows the profile obtained with bin 6 and Table 1 gives the width and displacement of the centre of the distributions obtained from the seven centre bins. The mean width of these distributions is 7.4 ± 0.4 mm and the centre is 2.9 ± 0.2 mm above the centre of the beam pipe.

The profile obtained includes the effect of multiple scattering in the vacuum pipe but the true beam height (h) can be estimated using $h^2 = h^2_{measured} - h^2_{scat}$. This gives a true beam height of 5.1 mm but can only be regarded as an estimate because of the lack of a precise knowledge of the momentum distribution and therefore the multiple scattering.

Conclusions

A beam profile monitor can be made using scintillation counters but its results will only be of use for luminosity measurements if the multiple scattering in the vacuum pipe can be reduced. In the measurements described the effective thickness of the vacuum chamber wall was 6 mm of stainless steel. This must be reduced by at least a factor of ten to make the effects of multiple scattering unimportant.

It was not possible to obtain a profile with normal gas conditions but this may have been due to the high background conditions when the attempts were made. The background was typically 100 times the calculated beam-gas background. However, great care will be needed to reduce the effects of randoms and showers and it will only be possible to produce an average profile over a long period of time.

* * *

Table 1

Summary of Beam Profile Data

Beam 1 600 mA 15 GeV Run 41'

Element	Total Width Half-Height (mm)	Displacement (mm)
4	7.1	3.1
5	7.2	2.6
6	7.7	2.8
7	7.6	3.0
8	8.0	3.2
9	7.4	2.8
10	7.0	2.7
Mean	7.43 ± .4	2.9 ± .2

Table 2

Legend Profile Monitor

H_1 Hodoscope # 1, 7 overlapping scintillators (11 → 17) forming 13 bins. Each scintillator is 6 × 5 × 300 mm.

H_2 Hodoscope # 2, 7 overlapping scintillators (21 → 27) forming 13 bins. Each scintillator is × 6 × 5 × 300 mm.

SC Scintillator placed between H_1 and H_2, covering the area of H_1 and H_2.

$\check{C}$ Čerenkov counter, 300 × 200 × 80 mm, Filling FC 75, $\beta_{thresh} = 0.78$.

V Veto counter, to shield against background from more than ~ 3 m upstream.

S Shaper.

D Delay.

GD Gated Dual Coincidence.

GA Gate.

DU Dual Coincidence.

Logic H_1 Logical mixer with output for any two or more (out $\geq$ 2) and for any three or more (out $\geq$ 3).

IV. SINGLE TELESCOPE DATA AT LARGE ANGLES

British/Scandinavian/CERN Collaboration.
(V. Agoritsas, B. Alper, K.M. Potter)

a) Background Tests

In order to examine the directional properties of the background radiation at I4, measurements were carried out with a scintillator telescope.[1] This consisted of 3 plastic scintillators 3 cm × 3 cm × 1 cm, with air light guides, separated by a distance of 7.6 cm. Signals were taken in triple coincidence with 8 ns resolving time. The telescope was mounted on a remotely controlled, rotating and traversing table.

The first run was carried out with the telescope in position A as shown in Fig. 15. There were steady circulating beams of 15 GeV/c and ~ 700 milliamp in each ring. The resulting count rate as a function of the angle between the telescope and beam 1, is shown in Fig. 16a. Most of the counts are attributed to beam-gas or beam-pipe interactions from ring 1. The contribution from beam-beam events, which would contribute to the 10° point in the figure, is expected to be small. The rise in the background above 90° is probably due to radiation from ring 2. This ring, according to the counters surrounding the downstream arm, was noisier than ring 1, during this run, by nearly an order of magnitude.

The dependence of the background rate as a function of distance from the pipe was also measured. Unfortunately the available range of movement was small. With the telescope inclined at ~ 9° to ring 1, 106 counts were recorded at a distance of 81 cm from the pipe and 75 counts were recorded at 112 cm from the pipe for the same length of time. This is consistent with a $1/r$ dependence for the background rate as a function of distance from the pipe.[1]

For comparison, the angular dependence of the background was remeasured when there was a circulating beam of 22 GeV/c in ring 1 only. For this run, the telescope was placed at position B of Fig. 15 and the middle element of the telescope was replaced by a larger, 10cm × 10 cm × 1 cm scintillator. The result of an angular scan is shown in Fig. 16 b. The curve is very similar in shape to the previous run, peaking around 9° to the pipe, though the fall-off at larger angles is marginally sharper.

1) V. Agoritsas et al., CERN/71-1.

It appears that at the ISR most of the background radiation is due to small angle beam-gas or beam-pipe interactions. Large angle radiation or general isotropic background levels are very small.

Detection of Large Angle Beam-Beam Interactions

As working conditions at the ISR improved, attempts were made to use the telescope to detect beam-beam events at large angles by scanning it through the intersection region. The use of a single arm device to detect beam-beam interactions above background is a problem directly relevant to many of the ISR experiments.

The telescope was left in position B, Fig. 15, but the scintillators were separated to a distance of 32.5 cm between the front and back counters in an attempt to reduce background from particle showers. In this position it subtended an angle of 36° to beam 2 from the intersection point.

On the night of 27th March, there were steady circulating beams of 15 GeV/c in the two rings. The currents were ~ 680 milliamp in ring 1 and ~ 515 milliamp in ring 2. The curve resulting from a 20° angular scan through the intersection region is shown in Fig. 17. The dotted line is a curve representing the background distribution. It is only an eye fit to the data but has essentially identical shape to the curve of Fig. 16a over the corresponding angular region. A clear excess of events occurs in the direction of the intersection region. This excess, normalised to 1 amp on 1 amp is 13 ± 4 events/100 sec. Using an effective luminosity of $3.5 \cdot 10^{27}$ as determined by the downstream counters, this represents about 5 times the expected rate from the thermodynamic model, though the signal to background ratio is too small, with the statistics available, to draw any reliable quantitative conclusions.

To improve the signal to noise ratio, the counters were separated further to a total distance of 42.5 cm in order to reduce further the probability of counting showers. In addition, the telescope was moved closer to the intersection to a distance of 165 cm and was moved to a larger angle (43° to beam 2) as the beam gas rate is expected to decrease faster at large angles than the beam-beam rate.

The run on the 8th April was at 22 × 22 GeV/c with intensities of approximately 1 amp circulating in each ring. Conditions were very clean.

In Fig. 18 the result of a wide angular scan is shown. The familiar background distribution, peaking at $\sim 7^{\circ}$ to ring 2, dominates, but now a clear secondary peak, at 43°, is visible. The curves are hand drawn eye fits to the data. The maximum beam-beam event rate from these curves is $\sim 10 \pm 2$ events/100 sec. Using a luminosity of 2×10^{28} as determined by the downstream counters, and also that the telescope could only see a maximum of $\sim 50\%$ of the intersection diamond, the rate is in excellent agreement with that of ~ 9 events/100/sec expected from the thermodynamic model.

During the same run a fourth scintillator $3 \times 3 \times 1$ cm was included in the telescope between the 10×10 cm counter and the rear one. The result of a detailed scan around the intersection region, with 4-fold coincidences is shown in Fig. 19. The single point, represented by a cross, under the peak was taken at the end of the run when only beam 2 was circulating and hence helps to estimate the background level under the peak. The beam-beam rate from this curve is 7 ± 2 events/100 sec, still in good agreement with the thermodynamic model.

Comparing Figs. 18 and 19, the background level under the beam-beam peak is seen to have fallen from ~ 7.5 to 4 events/100 sec with the inclusion of the extra scintillator. This suggest that a significant proportion of the background counts measured at large angles are due to showers rather than to through particles. The argument that this may have been due to a misalignment or inefficiency of the extra scintillator is ruled out since almost identical rates had been recorded at the 7° point. A much better signal to noise ratio can be anticipated with the more sophisticated experiments to be run at the ISR which could reject all showers.

In addition to the simple telescope rates, coincidences between the telescope and the downstream counters of ring 1 were recorded. The rates are represented by the black dots in Fig. 19. This trigger was found to be 100% clea . No counts outside the intersection region were recorded. The estimated event rate from the entire diamond was 3 ± 1 events/100 sec. Events which gave a triple coincidence between the telescope and both downstream arms were extremely rare. Only 4 such events were recorded in the entire run.

These studies indicate that with present conditions at the ISR, a simple single arm detector can measure beam-beam interactions with of the order of 30% background at large angles, and that essentially zero background can be obtained if an extra coincidence requirement is included.

V. TESTS WITH A NEUTRON TOTAL ABSORPTION SPECTROMETER

(Neutron production at Θ = 84 mrad)

CERN/Karlsruhe Collaboration.
(J. Engler, W. Flauger, B. Gibbard, F. Mönnig, K. Runge, H. Schopper)

A total absorption counter which had previously been used for total neutron cross section measurements at the PS was installed in intersection region I4 in order to get some information on background problems, the neutron production rate and possibly the neutron spectrum.

The layout is shown schematically in Fig. 20. The spectrometer S consists of a sandwich of 20 scintillators (40 × 40 cm^2) interspersed with iron plates (4 cm thick). The total thickness of 80 cm of iron corresponds to 6.5 interaction length which gives a practically 100% detection efficiency and an energy resolution of about ± 15% near 10 GeV/c. The counter was calibrated at the PS.

An anticounter A was used to suppress charged particles. However, coincidences with A were also recorded and hence a comparison between neutral and charged particles was possible.

An aluminium converter C (20 × 20 cm^2, 8 cm thick) was placed in front of the shower spectrometer and the trigger counter T was used to select events in which the hadronic cascade started in the converter. Since in this case edge effects are reduced a somewhat better energy resolution is obtained. On the other hand the detection efficiency for neutrons is reduced to only 6%.

The neutron counter was set up 9.5 m from the intersection and 80 cm from the beam, yielding an average angle of 84 mrad. The median plane of the counter was 20 cm above the beam line in order to reduce the amount of material traversed by the neutrons.

The neutron spectrometer was in coincidence with the two small angle telescopes described in section II (left L and right R, see Fig. 20), which were set up close to the beam pipes (Θ = 11 to 27 mrad). Each telescope consisted of an upper and a lower part. Data were taken separately

for the upper and lower halves of the telescopes. It was found that rates did not differ within the statistical errors.

The following trigger combination could be recorded simultaneously:-

for neutral particles $S\bar{A}$, L; $ST\bar{A}$, L ; $S\bar{A}$, R ; $ST\bar{A}$, R;
for charged particles STA, L; STA, R .

Coincidences with a telescope set-up at 90° (Strasbourg/Saclay group) were also taken. The rate for this trigger was two orders of magnitude lower than for the L trigger and thus the statistics are very poor. Analysis of this data is not yet complete.

The different trigger conditions were identified by a pattern unit. For each event the pulse height of S and the time of flight (t.o.f.) between L or R and S were written on magnetic tape. From the kinetic energy of the particle as inferred from the pulse height and the t.o.f. the mass of the particle was calculated for each event. The mass distributions were in agreement with the expectations taking into account the experimental resolutions. The uncertainty in the time measurement is mainly due to the longitudinal extension of the interaction diamond (about ± 2 nsec), whereas the energy resolution was impaired by rate dependent effects probably due to very low energy background. Hence a separation of n from π^0 and K^0 was not possible.

Beam-gas and beam-wall background

These background events could be separated from beam-beam interactions by comparing the counting rates for the beams properly crossing with those for the beams displaced or with only one beam. It was found that the counting rates of the neutron spectrometer alone ($S\bar{A}$, $ST\bar{A}$, STA) were almost completely due to background events. The same was true for coincidences with the R-telescope. The coincidences with the L-telescope on the other hand had very little background due to beam-gas or beam-wall interactions if the beam conditions were good. This could be observed most strikingly when the beam was circulating only in ring I.

The conclusion is that neutrons can be detected if the interaction is defined by another telescope for charged particles, whereas a single arm spectrometer for neutral particles seems to be very difficult to operate at least at small or intermediate angles.

π^0 and K^0 contamination

At an intermediate angle of 84 mrad, where the experiment was carried out, elastic scattering is very small and the relative K^0 production is not yet large. Indeed the thermodynamical model predicts that at this angle the K^0 intensity should be negligible compared to the neutron intensity except at very low energies. Hence, a distinction between K^0 and n did not seem absolutely necessary if we wanted to obtain only relatively crude rate and spectra data for the neutrons.

The π^0 intensities, on the other hand, according to the thermodynamical model, are likely to be comparable to the neutron intensities. In order to suppress γ's from π^0's most of the data were taken with 2 cm Pb in front of the anticounter. A run without lead showed no rate difference for neutron energies above 1.5 GeV. Below this energy the counting rate without lead rose steeply (Fig. 23). This shows that our neutron counter has very low sensitivity for γ's. Probably the reason is that most of the γ showers are absorbed in the Fe plates (2.2 radiation lengths thick) producing no or very little light in the scintillator plates. Hence we think that γ's from π^0's or other sources present no problem.

Luminosity measurements

During run 44 a luminosity curve was taken with the trigger ($S\bar{A}L$). The counting rate as a function of beam displacement is shown in Fig. 21. At the same time also the rate for charged particles was measured (STAL) and the result is shown in Fig. 22. Accidental coincidences have been subtracted in both cases. These results agree within the statistical errors very nicely with luminosity curves obtained by other groups in I4 , which indicates that we see beam-beam interactions.

The data taken during the run on 26.3.71 are also in excellent agreement with the data from other groups. They are not shown here since the luminosity run was not completed.

Neutron spectra

The neutron spectrum as derived from the pulse heights of S is shown for 15 GeV and 22 GeV colliding beams in Figs. 23 and 24 respectively. Above 4 GeV both spectra can be fitted by a straight line in a semi log plot over a wide range. The low energy deviation from this line which is toward an increased rate in all cases could be a result of a double scattering back ground discussed below. Of course, at the upper kinematical limit the spectrum has to go to zero. The spectrum at 22 GeV (slope 0.30 ± 0.03) seems to be somewhat flatter than at 15 GeV (slope 0.34 ± 0.03). This might simply be due to the higher kinematical limit at 22 GeV. The measurements are probably not accurate enough to draw a definite conclusion about the energy dependence of the spectrum.

At the intermediate angle of Θ = 84 mrad at which these data were taken the neutrons are thought to originate from "through going nucleons". Nucleons from $N\bar{N}$ pair production contribute very little. No predictions or measurements at lower energies exist for the neutron spectrum, but one would expect that it is not too different from the proton spectrum. The prediction for the protons as derived from the thermodynamical model (Hagedorn and Ranft) is shown in Fig. 23. The experimental resolution has been folded in. The predicted spectrum has a maximum at about 6 GeV which is not seen in the experimental spectrum. This might have two reasons. We found a large number of very low energy pulses (most of them below the electronic cut-off at 0.5 GeV) which caused a rate dependence of the energy calibration which might have smeared out the spectrum. However, this effect alone cannot explain the sharp rise at low neutron energies. This is probably due to particles originating from good beam-beam events which interacted with the wall producing a large number of low energy secondaries. Unfortunately this background cannot be separated out by the time-of-flight measurement. Only a thin vacuum chamber and additional anticounters could help.

Neutron rates

Because of the background effect mentioned above the spectra were integrated from 5 GeV upwards. In this range background corrections should be bearable. It was found that the number of neutrons $N(E > 5\ \text{GeV}) = 0.094/\text{sr}$

interaction at 15 GeV and 0.24/sr interaction at 22 GeV. These neutrons are in coincidence with forward going charged particles.

An at least crude comparison with theoretical predictions can be made in the following way. It is assumed that there is no correlation between the neutron and the charged particle. In view of the high average multiplicity this assumption should not be too bad. The solid angle and detection efficiency of the neutron spectrometer are well known (see above). The efficiency of detecting a charged particle in the L-telescope was given in section II. For non-colinear coincidence events the efficiency is approximately 0.5% at 15 GeV and 1.5% at 22 GeV. The efficiency of a single telescope is obtained by taking the square root again neglecting correlations. In this way one finds

Number of neutrons (E > 5 GeV)/sr interaction

	15 GeV	22 GeV
Experimental	1.3	2.0
Thermodynamic model (protons)	3.1	1.3

In view of the experimental and theoretical uncertainties the agreement is quite satisfactory.

Charged Particles

As has been mentioned above, data for charged particles were taken simultaneously by recording coincidences instead of anti-coincidences with counter A. The spectra obtained in this way are shown in Figs. 23 and 24.

Since p, π^+ and π^- cannot be distinguished the spectra are a sum of the spectra for all three particles. Nevertheless the shape of the spectra is very similar to those for the neutrons. The ratio of charged particles to neutrons is 2.5 at 15 GeV and 3.5 at 22 GeV. This seems to be the right order of magnitude since the total number of each p, π^+, π^- and n are comparable, and hence a ratio of about 3: 1 could be expected. The increase in the charge to neutral ratio from 15 GeV to 22 GeV also seems reasonable, as the increase in multiplicity would reflect primarily in an

increase in the number of π's, of which, as discussed above, we are sensitive at larger energies to only the charged ones.

Conclusion

1) A total absorption spectrometer for neutrons can be operated at the ISR. Secondary interactions in the walls should be reduced by thin beam pipes, anticounters or better geometry.

2) The total number of neutrons produced at an angle of 84 mrad agree within a factor of about 2 with the expectation.

3) The measured neutron spectrum disagrees with the predicted spectrum, but this could be due to a background from good beam-beam produced particles interacting in the walls. The spectra at 15 and 22 GeV are very similar.

4) The ratio of charged particles to neutron is about 3 : 1 at 15 and 22 GeV. The ratio of charged to neutrals seems to be increasing somewhat between 15 and 22 GeV.

VI. A GAMMA RAY ENERGY SPECTRUM AT 15°

CERN/Hamburg/Orsay/Vienna Collaboration.
(W. Schmidt-Parzefall, K.R. Schubert, M. Steuer and K. Winter).

Using a set-up with scintillation counters and a lead glass Čerenkov counter we looked for gamma rays during the five last nights before the ISR shut-down. We want to present here the results of the last night, 8th April, between 1 and 6 a.m. The set-up used during this time is shown in Fig. 25. Pulses from the lead glass photomultiplier were gated with the coincidence $(U_1 + D_1)(U_2 + D_2)\,\bar{A}R$ and then analysed by a 256-channel pulse height analyser. U and D are the small angle telescope counters described in section II (See Fig. 2). A is an anticounter, and R is the counter behind a 5.8 mm thick lead converter; this arrangement favours the detection of gammas to neutrons by a factor of 25. The energy spectrum obtained is shown in Fig. 26a.

The energy scale in this figure was determined by a calibration run with momentum analysed electrons in the b_{16} beam of the PS. Continuous checks at the ISR were possible using the 370 MeV line of minimum ionizing particles, gated by the coincidence BR. The vertical scale has been obtained with the parameters of table 1, taking into account the conversion probabilities in the beam tube and in the converter in front of R. The normalisation "per interacting proton" is in fact per $(U_1 + D_1)(U_2 + D_2)$, and it may well be that the fraction of diffractive events (giving no photons at 15°) in this trigger is much higher than $\sigma_{diff}/\sigma_{tot}$.

The main source of gamma quanta being probably π^0 decays, we have calculated the expected π^0 production spectra in the frame of the thermodynamical model of Hagedorn. Using the programme SPUKPC of J. Ranft, we took $N_{\pi^0}(E,\nu) = {}^1/_2[\,N_{\pi^+}(E,\nu) + N_{\pi^-}(E,\nu)\,]$ and simulated $\pi^0 \to \gamma\gamma$ decays at all π^0 angles and energies. The resulting energy spectrum of single gamma rays at 15° is shown in Fig. 26b ; a small correction for those cases where both gamma quanta hit the lead glass has been applied. The agreement between measured and expected spectra is good with respect to the shape but rather poor with respect to the absolute rate. Further measurements, e.g. varying the size of the trigger counters U, D and of the anticounter A, would be necessary before claiming that this difference is significant.

Table 1

Beam momenta	2×22 GeV/c
Beam currents	$I_1 = 1.00$ A, $I_2 = 0.95$ A
Running time	$t = 4.0$ h
Solid angle (of R) $\Delta\Omega$ =	2.3×10^{-3} sr
Counting rates: $S = (U_1 + D_1)(U_2 + U_2)$	= 561014
$\bar{S}AR$ =	1679
SAR =	8603 *)
$\bar{S}AR\check{C}$ = (E > 230 MeV) =	191

*) The ratio $\bar{S}AR/SAR$ is entirely compatible with $N_\gamma / N_{charged} = 1.0$, because 39% of all gamma quanta are preconverted in the beam tube (3 mm thick Fe assumed) and only 56% of the remaining quanta are converted in the Pb converter.

VII. TESTS WITH TWO MULTIWIRE PROPORTIONAL CHAMBERS

Split Field Magnet Detector Group
(F. Sauli).

Two multiwire proportional chambers have been recently installed in the I4 region and operated for a couple of weeks by our group. Though the main purpose of the installation was to test the MWPC system operation in the I4 environment, some of the results may be of general interest and are here summarized. All measurements refer to the following set-up:

a) Two MWPC, of active dimensions 38 x 38 cm^2 and 10 x 10 cm^2 respectively were placed at about 5 m from the intersect, between the two rings and very close to the downstream pipe of R1. The two chambers were about 5 cm apart.

b) A total of 128 wires had been equipped with electronics. This consisted of, per wire, a preamplifier with a gain of 10, a twisted cable connection, 60 m long, to the counting room and a line receiver with 50 mV of differential sensitivity. All wires in the same chamber were OR-ed together, to allow the singles and coincidence rate measurements.

c) The power and gas supplies were also placed in the counting room; we used the standard "Magic gas" with addition of 4% of Methylal.

The results of about two weeks of intermittent running can be summarized as follows:

1) The system operation was very satisfactory, despite the long connection between MWPC and counting room. In particular, even during the stacking procedure, no relevant noise was induced in the 60 m long unshielded signal cables (operating in the differential mode).

2) The efficiency of the chambers, as measured with a source, was constant with time.

3) The big "flash" of particles correlated with a dumping of the beam did not produce any detectable damage on the chambers. We intentionally ran the MWPC during the procedure defined as "Successive Accumulation and

Dumping in Ring 1", and we obtained several hundred "flashes" in the chambers. The typical flash produced 50 to 100 μA peak current in the HV supply of the chambers.

4) A short-lived induced radioactivity was detected after a long run, with a rate of ~5 coincidences/cm^2 sec after a dumping. The lifetime of this radioactive component is several minutes.

5) With 1.5 A circulating in R1 , a total interaction rate of ~ 10 coincidences/cm^2 sec was measured (mostly from beam/gas interactions) at about 30 cm from the ring.

VIII. PRELIMINARY MEASUREMENTS AT LARGE ANGLES

Saclay/Strasbourg Collaboration.

(M. Banner, G. Bassompierre, R. Morand, M. Schneegans, A.V. Stirling, J. Teiger, H. Zaccone, J. Zsembery)

During the March/April 1971 ISR runs, we performed some preliminary measurements of the interaction and background rates as well as time of flight and dE/dx spectra, with an array of counters, set up at 90° in the interaction region I 4.

VIII.1 Set-up

A telescope (see Fig. 27) of four counters: T, S, Hi and Ar, covering a solid angle of 22 msr, allowed us to measure single, double, triple and quadruple (signal F) coincidence rates at $(90 \pm 10)^\circ$. Two large anticoincidence counters A_1 and A_2 were shielding T and S from the beam halos. Counter A on the opposite side of the interaction region could be put in coincidence with signal F. Moreover, the signals S_1 and S_2 of the two small angle counter telescopes, described in section II, could be required in coincidence with signal F. Signal F also triggered the measurements of time of flight between counter T and AR and the recording of the pulse height distribution in counter H_3.

VIII. 2 Counting Rates

The rates are given without A_1 and A_2 counters in anticoincidence, as measurements during beam steering runs showed that they did not improve appreciably the ratio of beam × beam over background rates. The rates per second observed during two "quiet" runs respectively at 15 × 15 GeV and 22.5 × 22.5 GeV beam energies, are listed in the following table:

	15 GeV		22.5 GeV
I_1	1.507 A	0 A	1.005 A
I_2	1.439 A	1.439 A	0.954 A
T	550	389	285
S	9000	8465	1900
AR	17300	10977	3200
A_1	8300	6102	2430
A_2	20000	15220	5200
$A_1 * A_2$	4000	3382	1500
S*T	74	43	41
S*T*AR	13	4.6	8.3
$F=S*T*AR*H_i$	6.5	1.8	4.1
$S*T*AR*H_3$	1.3	0.37	0.84
$S*T*AR*(H_3)R$	0.005	0.002	0.0004
A*F	0.05	0.02	0.05
$S_1 * S_2$	29.1	0.75	41
$S_1 * F$	0.28	0.0	0.4
$S_2 * F$	0.30	0.07	0.4
$S_1 * S_2 * F$	0.014	0.0	0.5

During these stable measurements, the accidental rates were negligible ($\leq$ 1%). An order of magnitude of the beam x beam interaction rates can be obtained by subtracting twice the rate measured by the coincidence F when ring 1 was dumped, from the rate measured with two circulating beams: at 15 GeV in each beam, the beam× beam event rate at 90° is equal to ~ 3 particles per second for $I_1 \times I_2 = 2.2A^2$ and represents ~ 50% of the total measured rate. This value could be larger, due to the fact that beam 1 was much cleaner than beam 2. This rate is to be compared to the predictions of the thermodynamical model for the same current and solid angle conditions, which is 8 per second.

At 22 GeV in each beam, beam 1 was dumped only a few minutes before beam 2 and no reliable measurement with one beam could be obtained.

The rates of 90° events measured in coincidence with the small angle telescopes show clear evidence for beam x beam interactions though the statistics were low. The rate of coincidence $S_1 \cdot S_2 \cdot F$ is only 10^{-3} of the small angle coincidence $S_1 \cdot S_2$.

VIII.3 Time-of-Flight Measurements

Time-of-flight spectra at 15 GeV/c between counters T and AR are shown in Fig. 28. The absolute time calibration (0.4 nsec/channel) was done by putting counters T and AR close together and using a β source. The observed resolution (5.8 nsec) of the $\beta = 1$ peak is consistent with the size of the counters and the electronic resolution. No important contribution from prompt events is observed.

A spectrum with ring 1 dumped was recorded and normalized to two circulating beams. It can be seen that background interactions are mainly producing slow particles and it is confirmed that at 15 GeV/c they represent ~ 50% of the total rate.

VIII.4 The dE/dx Measurements

The pulse height spectra in counter H_3 (Fig. 29) obtained by triggering a) by particles with all velocities, b) by slow particles only, show good consistency between time-of-flight and dE/dx measurements.

VIII.5 Beam Steering

Attempts to put in evidence the beam x beam interactions at 90° by steering vertically the beams in I4 region did not succeed with our very preliminary set-up. As a beam x beam /background ratio of the order of 1/1 is observed when both beams are stable and quiet, any displacement in any intersection region causes the background to increase rapidly, thus hiding the decrease in beam x beam rate. If we ask the coincidence of the 90° telescope with both small angle telescopes, the statistics with a maximum of 10 minutes per measurement, were too low to obtain a clear peak.

IX. OBSERVATIONS WITH A LEAD-GLASS TOTAL ABSORPTION CERENKOV COUNTER AT 90°

CERN/Columbia/Rockefeller Collaboration.
(B. Blumenfeld, L. DiLella, M. Khachaturian, A. Placci, A.M. Smith, J.K. Yoh and E. Zavattini)

In preparation for experiment R-103 (search for dileptons at the ISR) we have made measurements of the rate and energy distribution of the background at 90°, using a total absorption lead-glass Čerenkov counter. The apparatus is shown in Fig. 30 (top view) and Fig. 31 (side view). S_1 and S_2 are plastic scintillators subtending a solid angle of 0.21 sr, provided by the Saclay-Strasbourg group (described in section VIII). Counters P_1 and P_2, also plastic scintillators, subtend a solid angle of 0.044 sr. Counter C is an SF5 glass cylinder 30 cm thick, 35 cm in diameter, seen by 7 58 AVP phototubes. Finally, plastic scintillator P_3 is used in coincidence with P_1 and P_2 for the purpose of measuring straight-through tracks in C which served for an energy calibration. The stability of the gain of counter C was monitored by the Am^{241} 5.3 MeV α peak in a CsI crystal located on the front face of the counter. A 1 cm thick Pb plate was located in front of P_2 to identify electrons by the larger pulse height in P_2 resulting from the shower produced. We indicate by P_2^* any signal from P_2 exceeding the level corresponding to twice that of minimum ionizing particles. Tests done at the Brookhaven AGS by some members of our group indicate that the $P_1 P_2^*$ coincidence should reject approximately 85% of the fast pions going through both counters.

During the run of April 5-6 at 15 GeV, we obtained the following rates:

Coincidence	Rate/sec × amp^2
$P_1 P_2$	6.9
$P_1 P_2 S_1 S_2$	0.08
$P_1 P_2^*$	1.3
$P_1 P_2^* S_1 S_2$	0.02

At the end of the run, beam 2 was dumped and we obtained the following rates

Coincidence	Rate/sec × amp^2
$P_1 P_2$	6.6
$P_1 P_2 S_1 S_2$	0.06
$P_1 P_2^*$	1.16
$P_1 P_2^* S_1 S_2$	0.01

A comparison of these two sets of results indicates that the main contribution to our counting rates comes from beam-gas or beam-wall collisions. It should be recalled that during this run the rate of beam loss was relatively high in both rings.

During the run of April 7 at 22 GeV, the following rates were measured

Coincidence	Rate/sec × amp^2
$P_1 P_2$	10
$P_1 P_2 S_1 S_2$	0.15
$P_1 P_2^*$	0.7
$P_1 P_2^* S_1 S_2$	0.01
$P_1 P_2 B_1$ or $P_1 P_2 B_2$	0.4
$P_1 P_2^* B_1$ or $P_1 P_2^* B_2$	0.03

where B_1 and B_2 are signals from the small angle telescopes relative to ring 1 and ring 2, respectively, which are described in section II. No measurement with only one circulating beam was possible.

For all runs, the energy distribution in counter C was consistent with an exponential of the type e^{-E/E_0}, where $E_0 \approx 300$ MeV independently of the coincidence used to gate the signal from counter C.

Gating C with the coincidence $P_1 P_2$, the following rates were obtained during the run of April 7 for various intervals of energy deposited in C :

Energy interval (GeV)	Rate/sec × amp^2
0.5 - 1	1
1 - 1.5	0.13
1.5 - 2	0.03
> 2	0.003

Under conditions more closely related to experiment R - 103, the rate of $P_1 \bar{P}_2^* S_1 S_2$ coincidences with an energy loss in C between 0.5 and 1.0 GeV was 0.005 sec^{-1} amp^{-2}, while no count above 1.5 GeV was observed in 80 minutes.

In conclusion, it appears from these measurements that all rates are low enough to enable the proper functioning of the apparatus being built for R - 103.

X. TEST EXPOSURES WITH NUCLEAR EMULSIONS

Bombay-Bucharest-CERN-Cracow Collaboration.
(H. Annoni, A. Cordaillat, O. Czyzewski, E.M. Friedländer et al., J. Gierula, A. Gurtu, A.J. Herz, P. Zielinski).

X.1 General

The purpose of the test exposures was to obtain information about background conditions and to gather operational experience with a set-up which resembled as closely as possible that proposed for full-scale physics runs. Part of the material has now been analysed and we give below a summary of results to date(7 May). Additional data are expected during the next few weeks.

X.2 Set-up

The nuclear-emulsion plates and stacks were transported from outside the shielding wall through a labyrinth to the exposure positions near the intersection region by means of a 16 mm (HO gauge) toy railway train, and returned by the same method. It was thus possible to ensure that the emulsions were exposed only when the beams were stable.

X.3 Exposures

Five sets of exposures were made in various positions near the intersection region. However, the results we present here were all obtained from two of the runs, and in each case from a stack of 10 cm × 5 cm Ilford K5 emulsions, 400 μm thick, placed close to the interaction region:

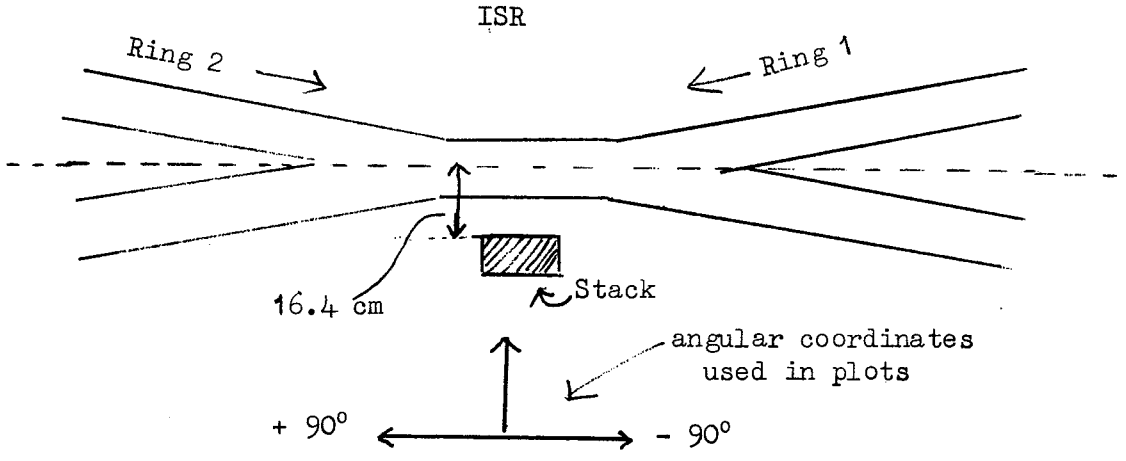

Details of exposures:

Date	Energy	I_1	I_2	Stack	Remarks
30.3.71	15 GeV	0.99 A	0.98 A	ISR2	Ring 2 background ~ 100× "expected"
8.4.71	22 GeV	1.00 A	0.95 A	ISR4	Ring 1 background ~ 2× "expected" Ring 2 background ~ 3× "expected"

The background estimates were based on the counting rates in the small angles telescopes described in section II.

X.4 Angular distributions

Fig. 32 shows the angular distribution of horizontal minimum-ionization tracks in stack ISR4 ; Fig. 33 shows the same distribution for stack ISR2 . The numbers of tracks counted in the range + 45° to + 90° which contains the ring-2 peak were made equal so as to allow a subtraction that might eliminate effects due to beam-wall interactions in ring 2. The result of the subtraction is shown in Fig. 34. It appears probable that most of the tracks between - 45° and + 45° in stack ISR4 are due to beam-beam interactions. The interaction diamond is expected to subtend an angle of ± 50° or so at the stack.

X.5 Gamma rays

Fig. 35 shows the angular distribution of electron pairs in ISR4 . It clearly has the same general shape as that of the minimum-ionization tracks.

X.6 Random background

The general radiation level in the interaction regions is so low as not to interfere in a serious way with emulsion exposures of the durations needed to obtain good data.

X.7 Background due to beam-wall and beam-gas interactions

It is clear from Fig. 32 and Fig. 35 that the fluxes of charged particles and photons along the beam directions are too high to allow the observation of the products of beam-beam collisions in the small angle region (± 45° to 90° in our coordinates). One may, of course, expect the

situation to improve with increasing luminosity, but it seems clear already that shielding will be required in addition. Inspection of Fig. 34 suggests that a simple background subtraction is unlikely to give reliable results unless statistics are very high and ISR conditions are controlled much better than they have been up to now.

X.8 Further data to be obtained

We do not yet have adequate data concerning the background of slow charged particles originating in beam-wall interactions. In addition we have to make tests to decide how much shielding will be required to reduce the background due to beam-wall interactions in ring 2 to an acceptable level, and where this shielding should be placed.

X.9 Conclusion

The data obtained in the first two weeks of analysis suggest strongly that all the emulsion experiments proposed are feasible in the large-angle region (between -45° and $+45^{\circ}$ in our coordinates) as long as the ISR performance is comparable to the best obtained up to now, and exposure times are adjusted to take account of luminosity.

To make measurements in the small-angle region (45° to 90° in our coordinates) shielding will be needed to remove the halo accompanying beam 1.

We do not yet have adequate data on the background of slow charged particles produced in beam-wall and halo-wall interactions in the vicinity of the interaction region.

XI. TESTS OF A COUNTER TELESCOPE TO BE USED IN A SEARCH FOR QUARKS

CERN-Munich Collaboration

(M. Bott-Bodenhausen, C. Fabjan, C. Gruhn, B.D. Hyams, L. Peaks, U. Stierlin, B. Winstein).

Introduction

During the recent ISR physics run (April 1971), the CERN-Munich quark search experiment conducted preliminary measurements in order to determine the amount of background and other spurious contaminations. The basic telescope consisted of nine small counters (five counters 10 × 10 × 1 cm; four counters 9 × 9 × 1 cm of a Nuplex plastic) situated directly underneath ring I and virtually touching the vacuum pipe at a distance 4 m from the diamond. The experimental arrangement together with anticounters and light guide positions is shown in Fig. 36. Telescopes U_1 U_2 D_1 and D_2 of the small angle telescope described in section II were also used at times in the trigger to select beam-beam signals.

Luminosity Measurements

Luminosity measurements were taken as the two beams were displaced vertically with respect to each other during ISR run # 44. A plot of the number of beam-beam coincidences is shown in Fig. 37 using both a double and a triple arm coincidence. Fig. 38 shows the nine-fold coincidence rate as a function of beam position in ring I. The effect of beam wall collisions is seen dramatically. The rates in Fig. 37 and Fig. 38 represent counts over a seven minute period.

In addition to this, random rates were simultaneously monitored for two and three arm triggers, and these are summarized in the following table:

Pos. of I Pos. of II	9 Fold + U 2	9 Fold + U2 delayed	9 Fold + U1 + U2	9 Fold + (U_1+U_2) delayed
+ 0.5 - 0.5	1.2×10^3	1.9×10^2	26	0
+ 1.5 - 1.5	5.6×10^2	2.0×10^2	7	0
- 0.5 + 0.5	1.7×10^3	1.9×10^2	26	1
- 1.5 + 1.5	1.5×10^3	2.6×10^2	35	0
- 2.5 + 2.5	410	15	15	0
+ 1.5 + 2.5	1.3×10^3	0	24	0

Table XI-1 : Counts over 7 minute periods. Current in ring I 666 mA. Current in Ring II ~ 840 mA. Delayed pulses were delayed by 100 nanoseconds.

From these figures and graphs we can conclude the following:

a) The effective beam height was roughly 4 mm.

b) A three arm coincidence yields a very clean beam-beam signal, even when the background rates are high.

Preliminary Quark Search

Under test-beam conditions (d_{30a}) a 9 scintillator telescope with appropriate anti-counters yielded a rejection factor of better than 10^{-9} (ISRC 71-8/Addendum 1). However, for our early runs in the ISR, virtually the same system had a rejection factor of about 10^{-5}. That is, one out of 10^5 9 fold coincidences have low pulse heights, in the charge $^1/_3$ region, in all 9 counters. These low pulse heights we know to be due

to Čerenkov radiation from particles in the light guides (plexiglas). We attribute the poorer rejection to particles coming from more than one direction (into the guides) and possibly to showers in the wall of the vacuum chamber sending a spray into the light guides. In our final set-up we will probably use light guides made of scintillator material to minimize this situation.

We photographed the 9 pulses on an oscilloscope for all "candidates" in $\sim 10^4$ beam-beam collisions, defined by our 9-fold in coincidence with the telescope U_2.

Up to now, we can say that we see no quarks in $\sim 10^4$ beam-beam secondaries at ~ 20 milliradians.

ACKNOWLEDGEMENTS

In addition to the names at the head of each section a large number of other people worked hard to make the measurements in I4 possible. As mentioned in the Introduction, the authors are particularly grateful to all the staff of the ISR as well as many other members of their own groups.

G. Sicher, R.H. Watson and L. Velati gave valuable assistance with the installation of equipment and we are grateful to F.F. Heymann, M. Gibson, P. Sharp, L. Carrol, V. Smith, G. Barbiellini, F. Niebergall and M. Regler for help and advice. The authors of section X would also like to thank U. Brotschi and O. Mendola as well as the microscopists at CERN, Bucharest and Cracow.

FIGURE CAPTIONS

Fig. 1 - Record of the observations made on 27 January, 1971, when both beams circulated in the ISR for the first time. (Telex to B.P. Gregory, then at Brookhaven National Laboratory, USA).

Fig. 2 - a) Betatron envelope of the undisplaced beam (arbitrarily taken to be 14.5 mm high) in the vicinity of an intersection. Closed orbit distortions have been ignored.

b) Closed orbit bump produced by the steering magnets, arbitrarily taken to be 7.2 mm in the intersection.

c) Envelope of the displaced beam. Data scaled from E. Keil and P. Strolin, (CERN/ISR-TH/70-8. (S = steering magnet, F,D = Focusing (defocusing) magnet, T = Terwilliger quadrupole).

Fig. 3 - Arrangement of counters used for the "small angle" luminosity data. Size in mm.

Fig. 4 - Luminosity data at 22.5 - 22.5 GeV, for the combination (U_1 OR D_1) AND (U_2 OR D_2). Open points indicate data taken with $I_1 = 0.71$ A, $I_2 = 0.071$ A, closed points refer to $I_1 = 1.28$ A, $I_2 = 0.071$ A.

Fig. 5 - Luminosity data at 22.5-22.5 GeV for the combinations UU, DD, UD and DU. Open points at $I_1 = 0.71$ A, $I_2 = 0.071$ A, closed points at $I_1 = 1.28$ A, $I_2 = 0.071$ A. The vertical scales cannot be compared (see text).

Fig. 6 - Luminosity data at 15.3-15.3 GeV, for the combination UU, DD, UD and DU. Open circles with centre line of the two beams at z = 0, closed circles with centre line at + 2 mm. $I_1 = 0.662$ A, $I_2 = 0.837$ A.

Fig. 7 - Rates in the single telescopes U_1 and D_1 versus vertical displacement of beam I.

Fig. 8 - Rates in the single telescopes U_2 and D_2 versus vertical displacement of beam II.

Fig. 9 - Rates in the telescopes in intersection I4 versus beam displacements in intersection I5 .

Fig. 10 - Rates in UD versus the current product $I_1 \times I_2$. The solid line indicates the rate expected for a constant effective height.

Fig. 11 - Time-of-flight spectrum between the small angle telescopes on opposite downstream arms.

Fig. 12 - Schematic plan of the arrangement of hodoscopes and counters of the beam profile monitor.

Fig. 13 - Diagram of the logic of the beam profile monitor.(For legend see Table II Section III).

Fig. 14 - Beam profile of a 600 mA 15 GeV beam in ring 1 on 26/3/71 (element 6).

Fig. 15 - Position of the single arm telescope in I4 .

Fig. 16 - Angular distribution of the background
a) in position A of Fig. 15
b) in position B of Fig. 15.

Fig. 17 - The telescope counting rate as a function of angle when pointing at or around the intersection point with 15.3 GeV colliding beams (I_1 = 680 mA I_2 = 515 mA, 17/3/71).

Fig. 18 - The telescope counting rate as a function of angle with 22.5 GeV colliding beams (I_1 = 1 amp I_2 = 1 amp, 8/4/71).

Fig. 19 - Counting rate of the fourfold telescope when pointing at the intersection with 22 GeV colliding beams (I_1 = 1 amp; I_2 = 0.95 amp).

Fig. 20 - The position of the neutron total absorption spectrometer.

Fig. 21 - A luminosity curve obtained with neutral particles, trigger $\bar{S}\bar{A}L$.

Fig. 22 - Luminosity curve obtained with charged particles, trigger STAL.

Fig. 23 - Neutron spectrum with 15.3 GeV colliding beams.

Fig. 24 - Neutron spectrum with 22.5 GeV colliding beams.

Fig. 25 - Arrangement of scintillation counters and lead-glass Čerenkov counter used to detect gamma rays.

Fig. 26 - Energy spectrum of gamma rays at 15°
a) Experimental results with 22 GeV/c colliding beams
b) Spectrum calculated from the thermodynamical model of Hagedorn.

Fig. 27 - Arrangement of counters to detect large angle particles.

Fig. 28 - Time-of-flight spectra between counters T and AR with 15.3 GeV colliding beams.

Fig. 29 - Pulse height spectra
a) of particles with unselected velocity
b) of slow particles only.

Fig. 30 - Plan view of the arrangement of the total absorption Čerenkov counter at 90°.

Fig. 31 - Side view of the arrangement of the total absorption Čerenkov counter at 90°.

Fig. 32 - The angular distribution of horizontal minimum-ionization tracks in stack ISR 4.

Fig. 33 - The angular distribution of horizontal minimum ionization tracks in stack ISR 2.

Fig. 34 - Difference between ISR 4 and ISR 2 normalized to give equal numbers between +45° and +90° (Ring 2).

Fig. 35 - Gamma-ray angular distribution in plate 2 of stack ISR 4.

Fig. 36 - The experimental arrangement of the quark search scintillation counter telescope.

Fig. 37 - Beam-beam coincidences as a function of beam displacement.

Fig. 38 - Counting rate of the ninefold coincidence as a function of beam position in ring I.

22107a rsge ch
23698z cern ch

geneve/rsg/telex23698/210 29.1.71 1605hrs

lt
prof. b. gregory
guesthouse
brooklab
upton. l.i. ny/usa

observation beam-beam collisions in intersection no. 4 at isr.
on 27/1 13:25 hours, about 2 hours after
startup of isr physicists working in intersection 4
observed first events which could be identified with high
probability as resulting from collisions in i-4 between
two proton beams in the rings.
ten events were observed in 640 sec. the calculated rate of
accidental events was 0.3 in same period of time stop
equipment consisted of three counters above downstream arm of
beam 1 and three counters below downstream arm of beam 2.
about 6 hours later, when a new period of stable conditions had
set in, with about 2.5 amp in ring 1 and 23 ma in ring 2, 105
coincidences were observed in 1400 sec. while measured rate of
accidental events over same period was 11. after dumping beam 2,
both rates went down to zero counts in 100 sec. the measurement
was repeated with 2.2 a in ring 1 and 80 ma in ring 2, 212 coinci-
dences as against 72 accidentals were recorded in 1000 sec. these
data thus show unambiguously that beam-beam collisions have taken
place in isr stop the numbers are in rough agreement with rate
expected from currents in rings and geometry of the equipment and
rate of events scales roughly as product of two currents stop
the team is composed of one or two physicists of essentially
all groups that are now preparing experiments for later in the
year.
the go-ahead to do these measurements was given one week earlier,
by isr committee in meeting 20 january

sens cernlab

22107a rsge ch
23698z cern ch

u

Fig 1

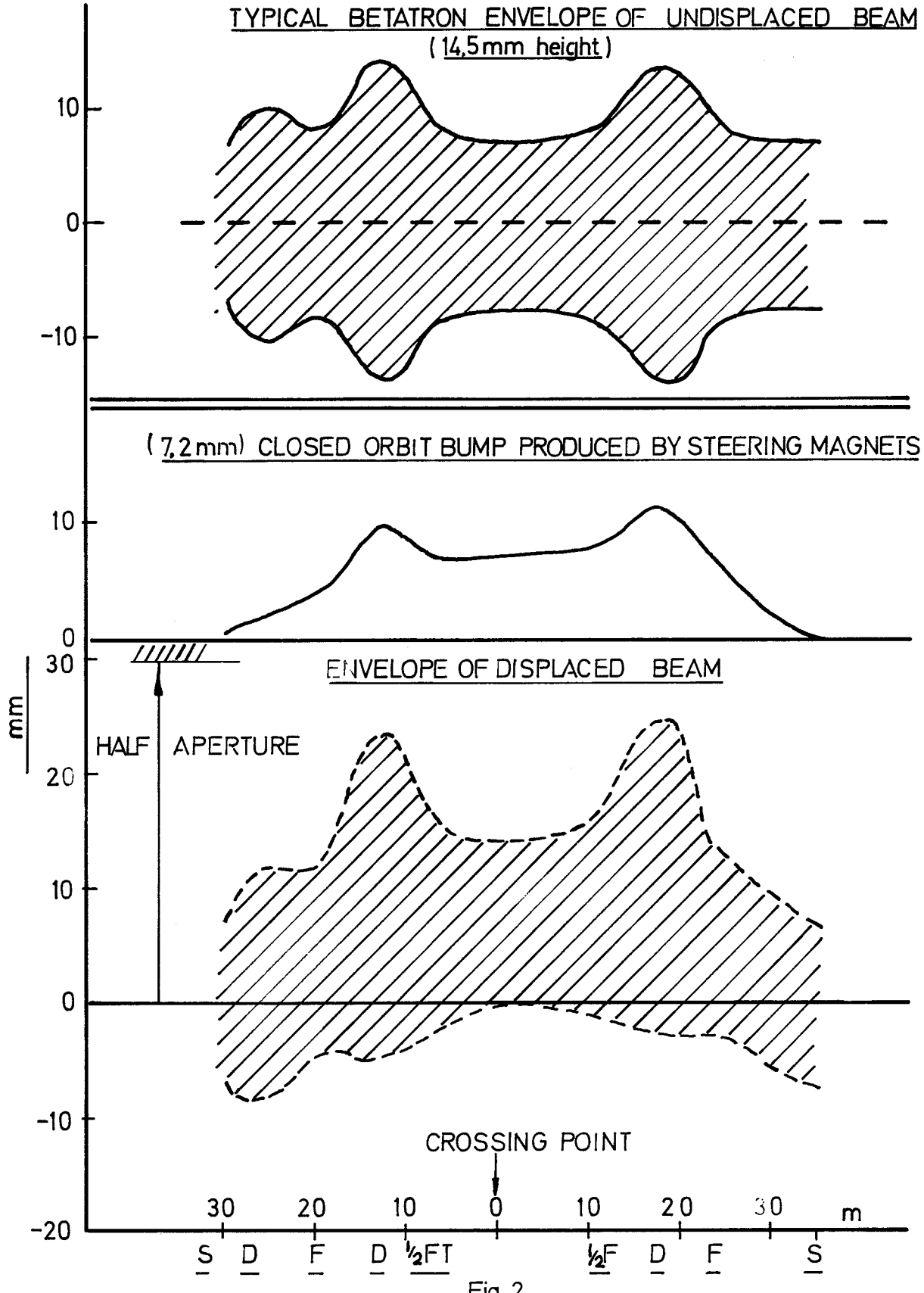
TYPICAL BETATRON ENVELOPE OF UNDISPLACED BEAM
(14,5 mm height)
10
0
-10
(7,2 mm) CLOSED ORBIT BUMP PRODUCED BY STEERING MAGNETS
10
0
ENVELOPE OF DISPLACED BEAM
mm
30
HALF APERTURE
20
10
0
-10
CROSSING POINT
-20
30 20 10 0 10 20 30 m
S D F D ½FT ½F D F S

Fig. 2

THE SMALL ANGLE TELESCOPE ARRANGEMENT IN I 4

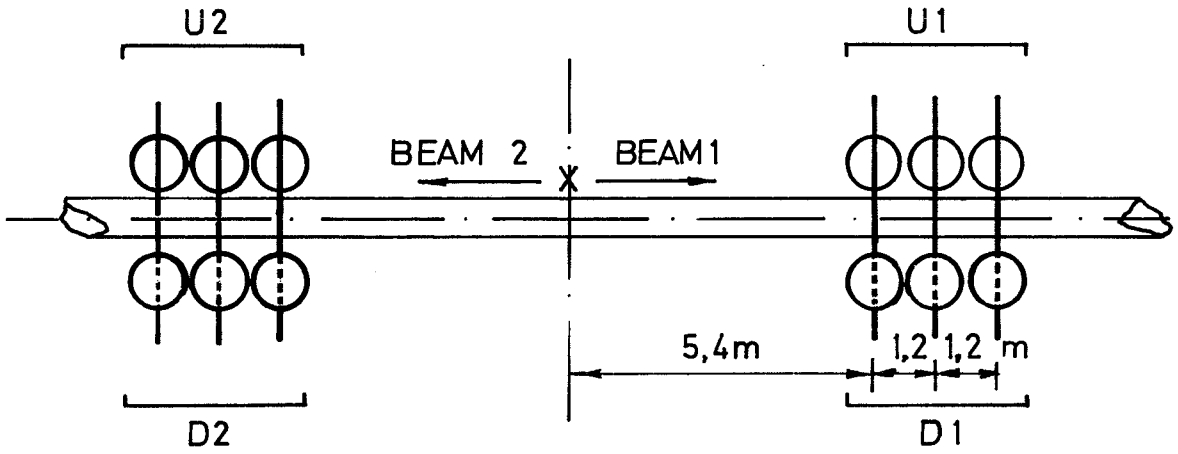

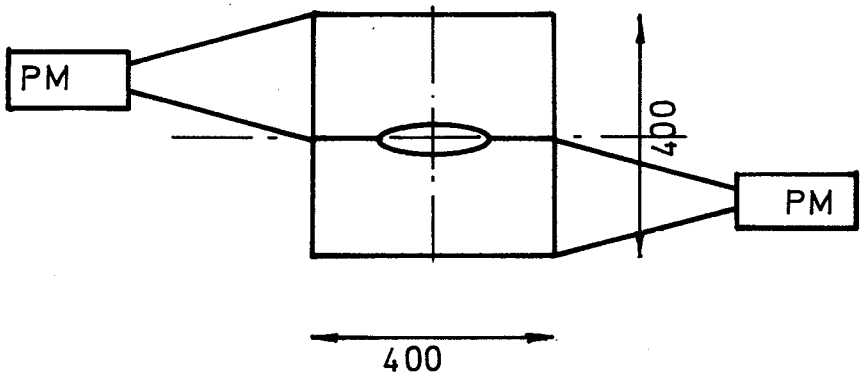

Fig 3

ISR LUMINOSITY AT 22,5 GeV / 22,5 GeV

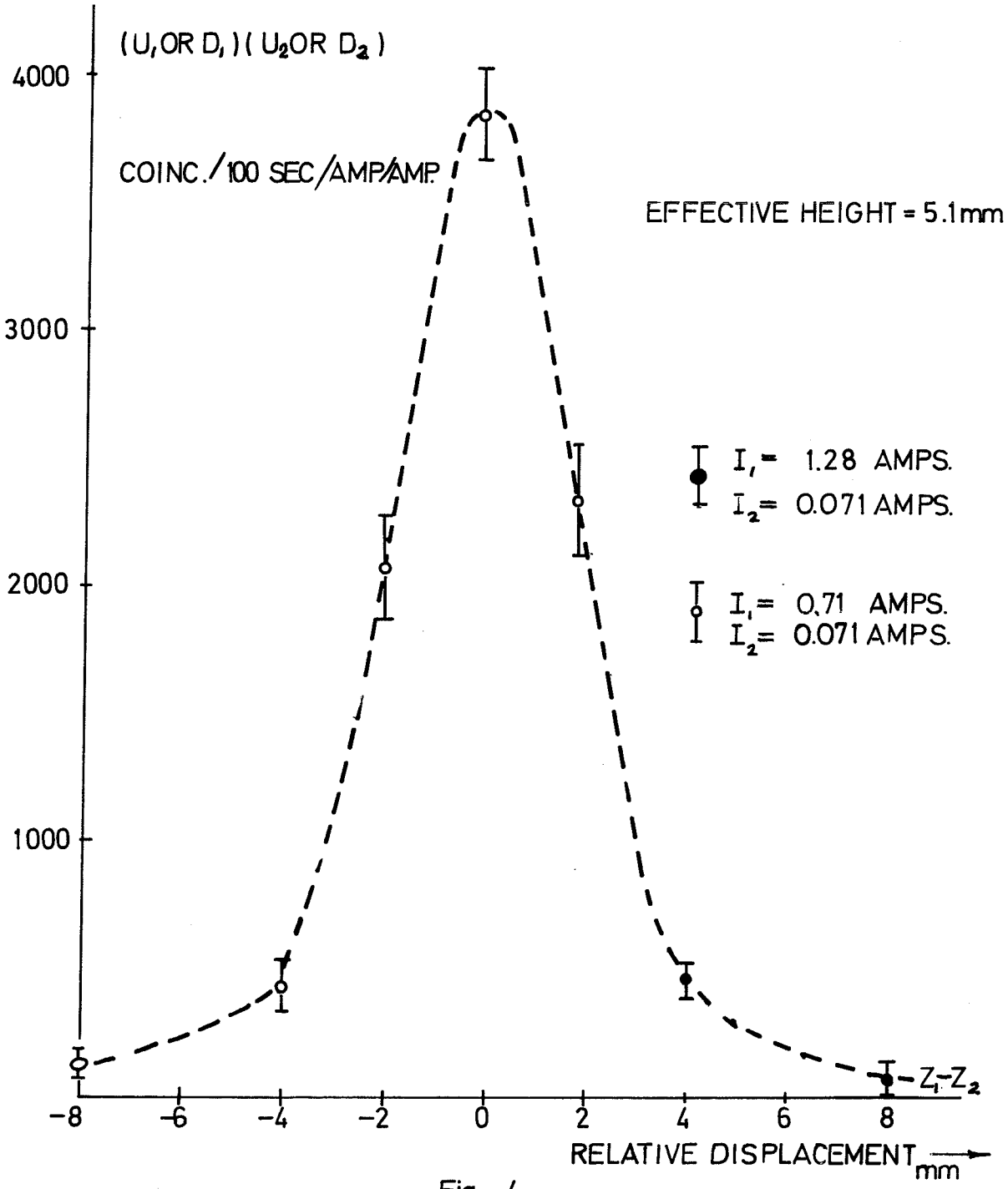

Fig. 4

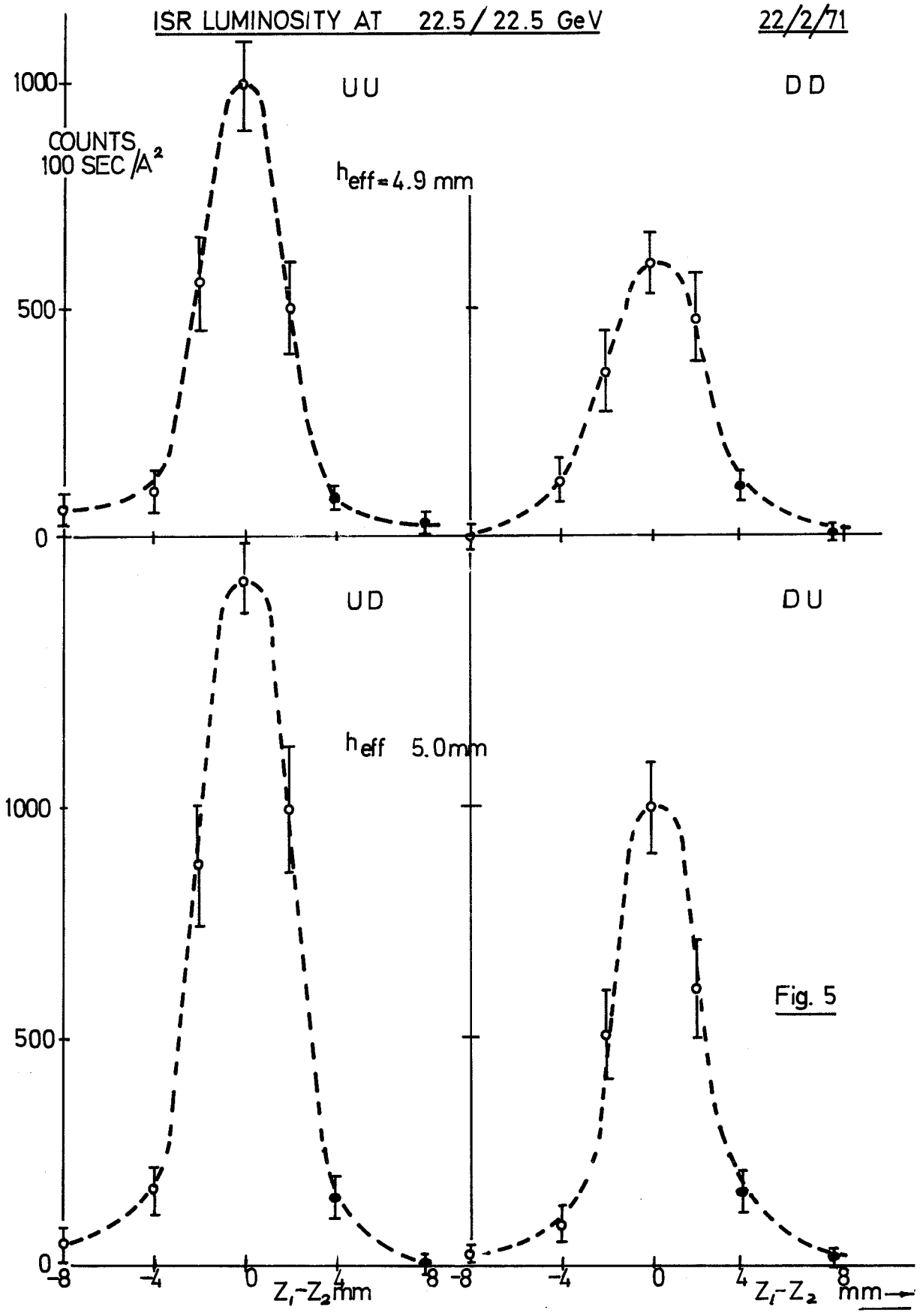
ISR LUMINOSITY AT 22.5 / 22.5 GeV
22/2/71
UU
DD
UD
DU
COUNTS
100 SEC /A²
h_eff = 4.9 mm
h_eff 5.0mm
1000
500
0
-8
-4
0
4
8
Z₁-Z₂ mm
Z₁-Z₂ mm

Fig. 5

ISR LUMINOSITY AT 15.3 / 15.3 GeV 5/4/71

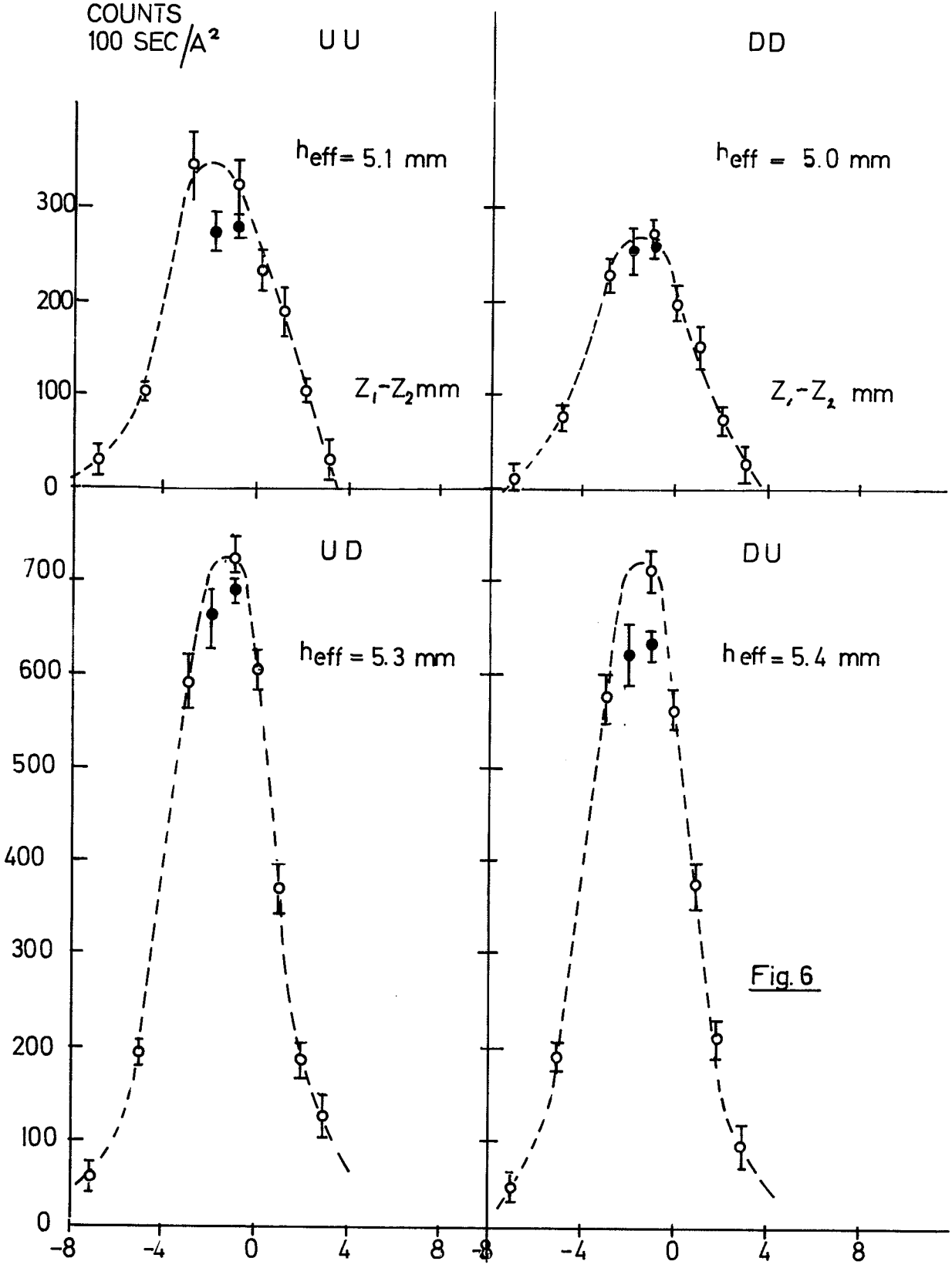

Fig. 6

LUMINOSITY DATA I 4

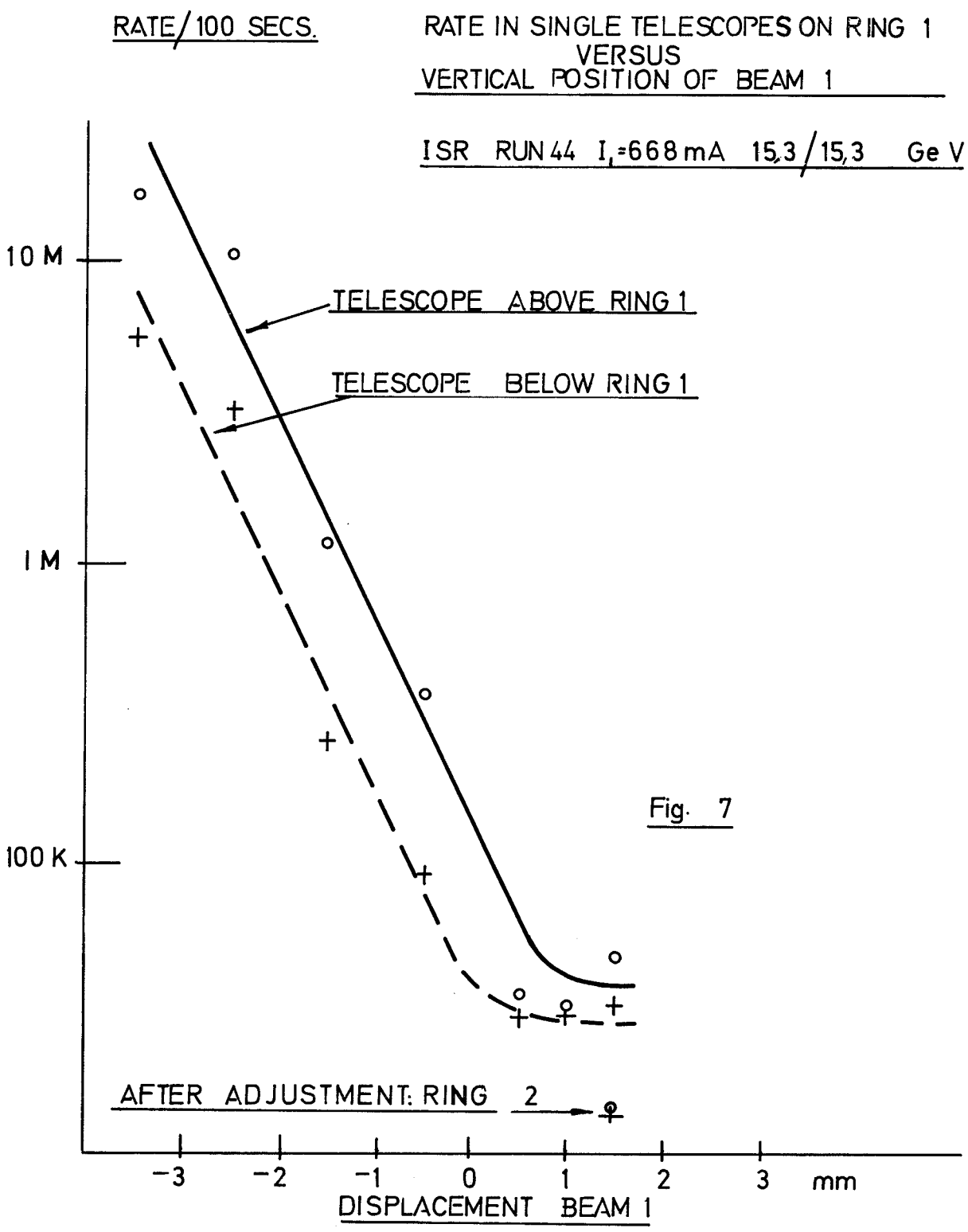

Fig. 7

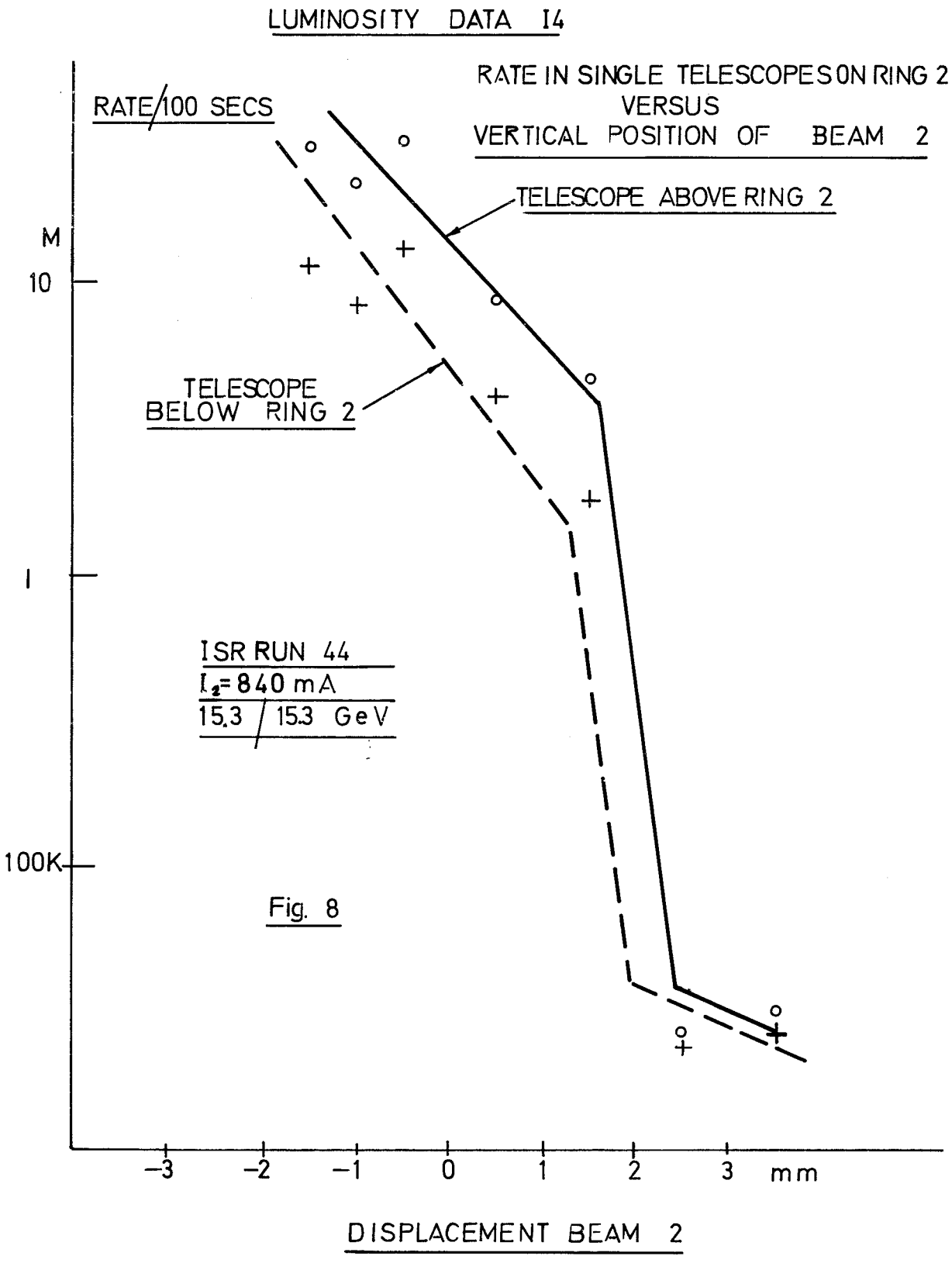
LUMINOSITY DATA I4
RATE IN SINGLE TELESCOPES ON RING 2
VERSUS
VERTICAL POSITION OF BEAM 2
RATE/100 SECS
TELESCOPE ABOVE RING 2
TELESCOPE
BELOW RING 2
M
10
1
100K
ISR RUN 44
I_2 = 840 mA
15.3 / 15.3 GeV
−3
−2
−1
0
1
2
3
mm
DISPLACEMENT BEAM 2

Fig. 8

EFFECT OF BEAM DISPLACEMENT
IN I 5 ON COUNT RATES IN I 4

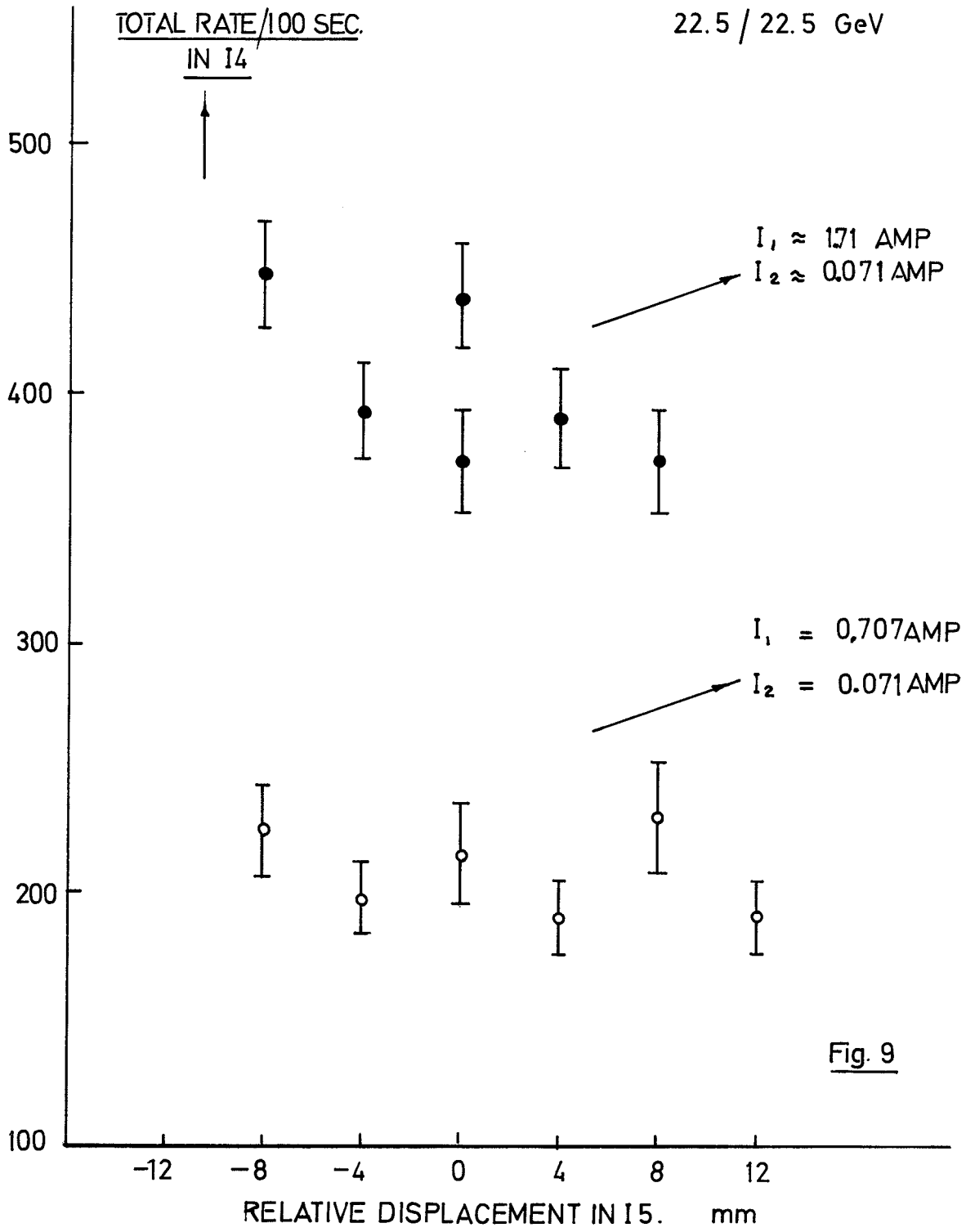

Fig. 9

VARIATION OF EFFECTIVE HEIGHT WITH TIME 5/4/71

U D EVENTS/1000 SECS RUN 44 15.3/15.3 Ge V

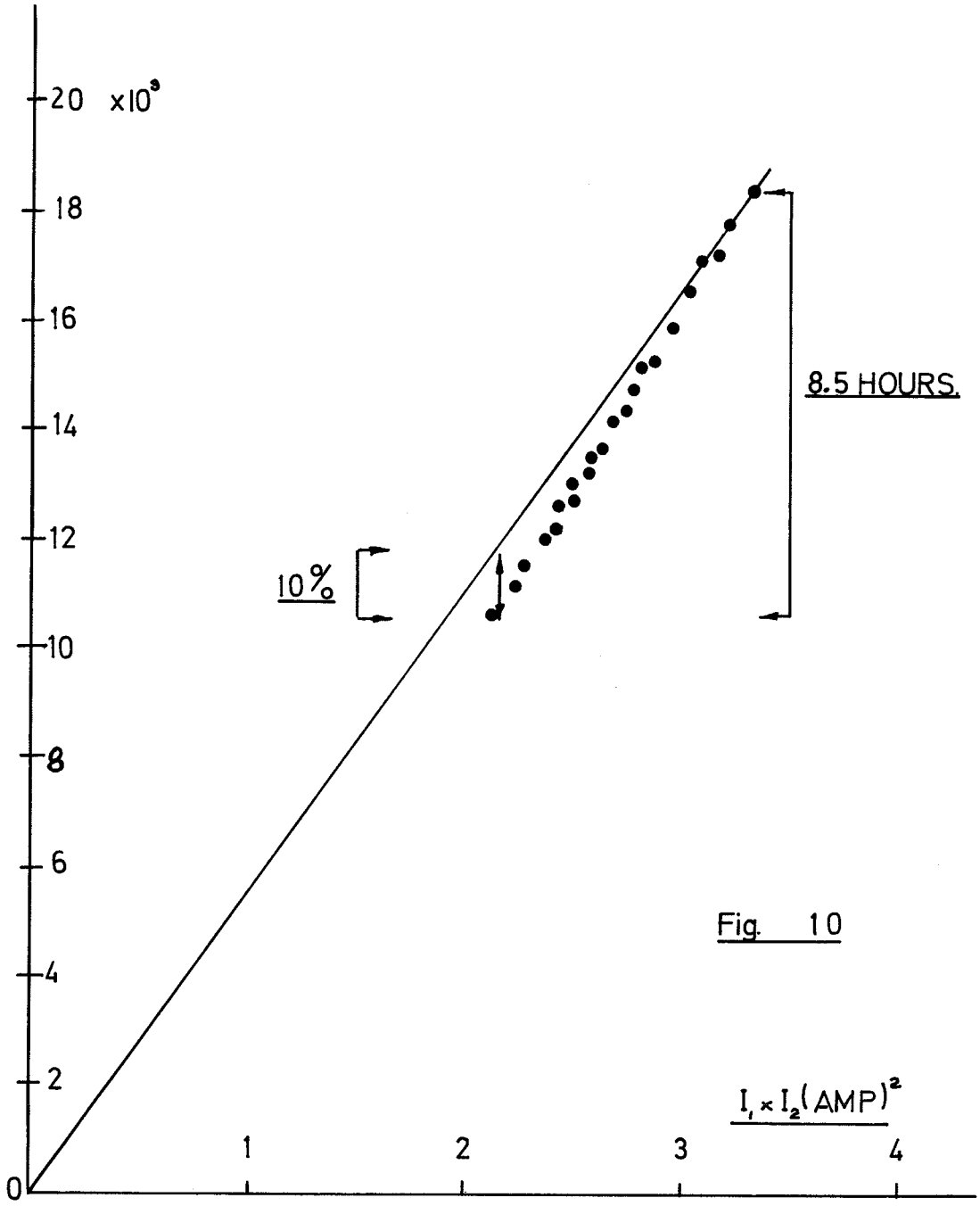

Fig. 10

TIME OF FLIGHT SPECTRUM I 4 17/2/71

(SMALL ANGLE TELESCOPE)

22.5 / 22.5 Ge V

I_1 = 2.158 AMP

I_2 = 0.095 AMP

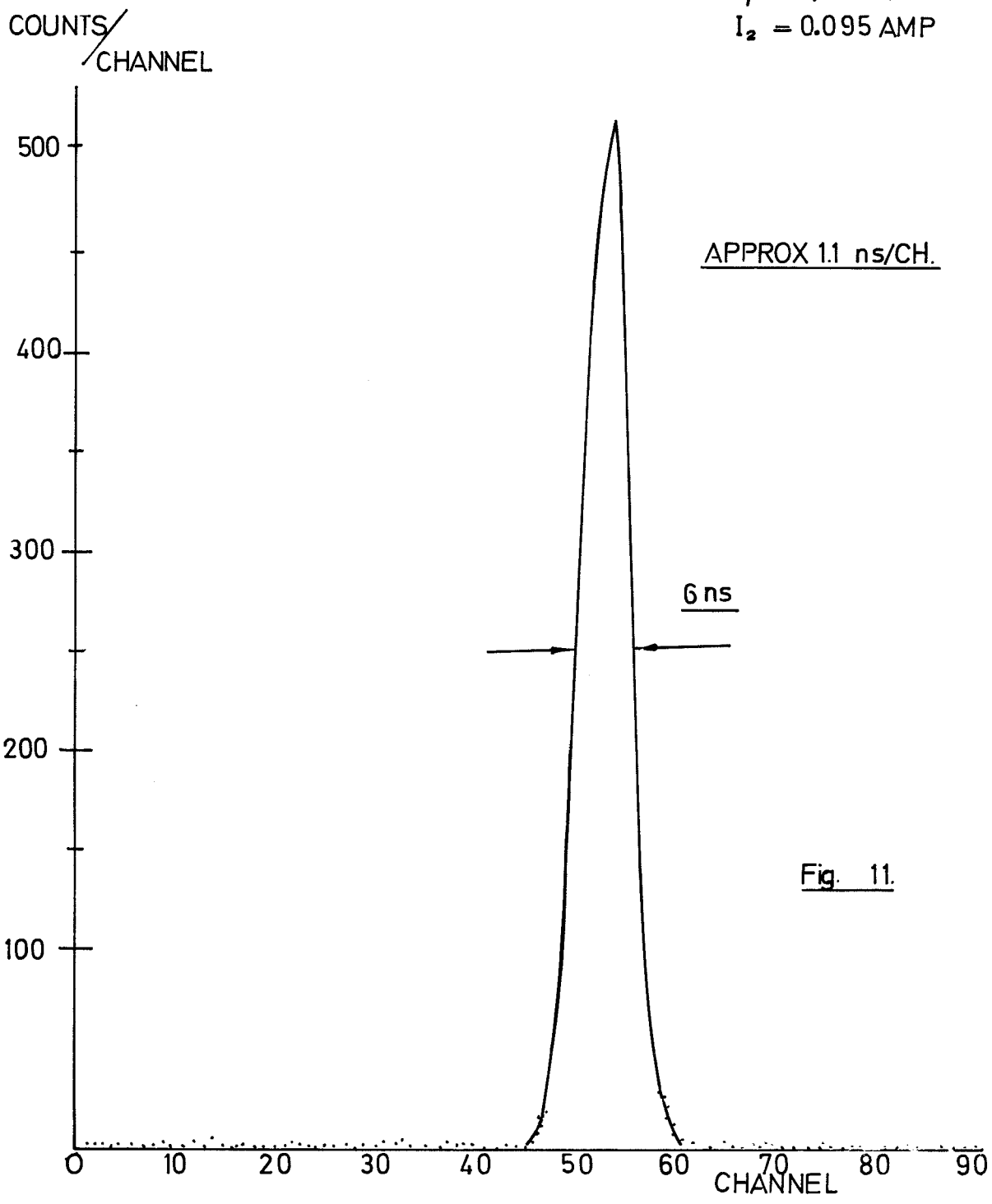

Fig. 11.

BEAM PROFILE MONITOR

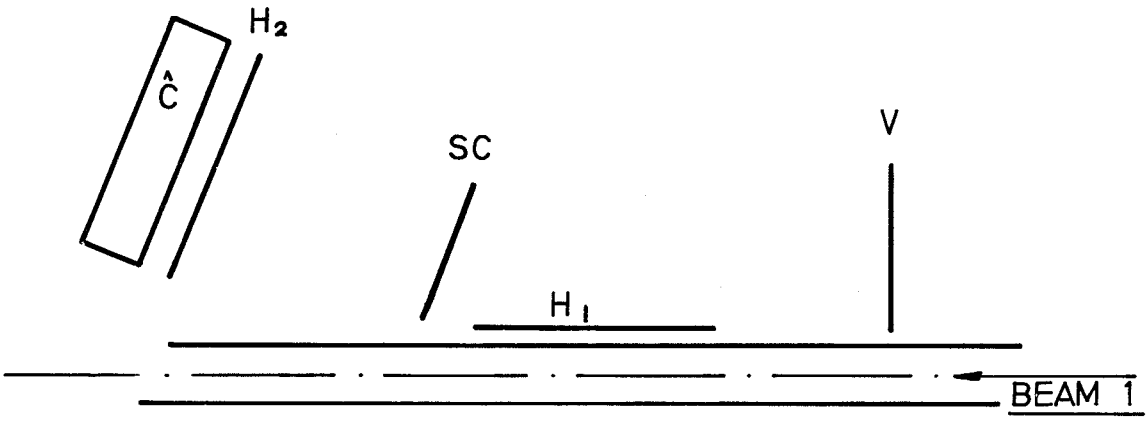

FOR LEGEND SEE TABLE II SECT. III

Fig. 12

PROFILE MONITOR LOGIC DIAGRAM

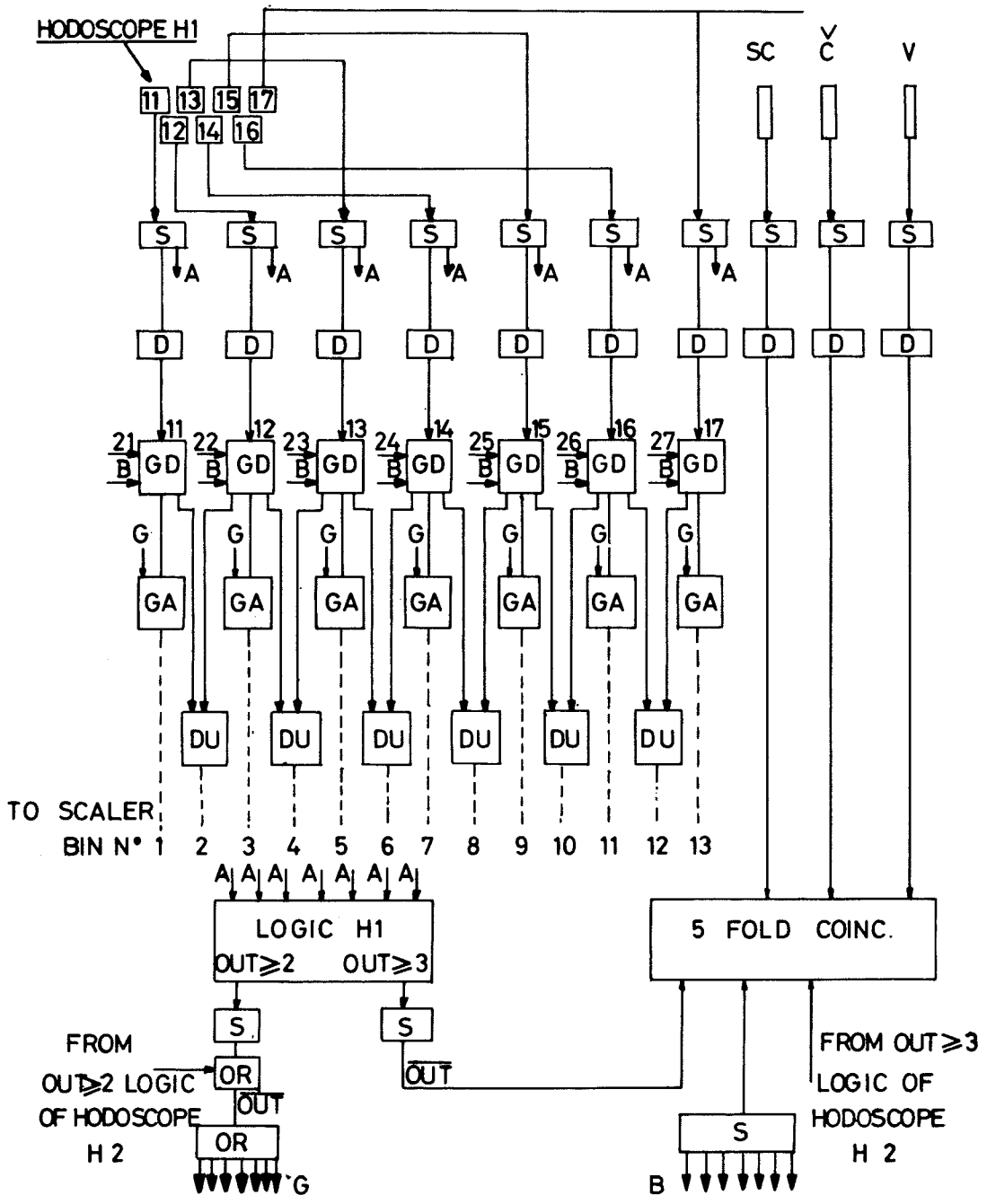

FIG 13

BEAM PROFILE BEAM 1

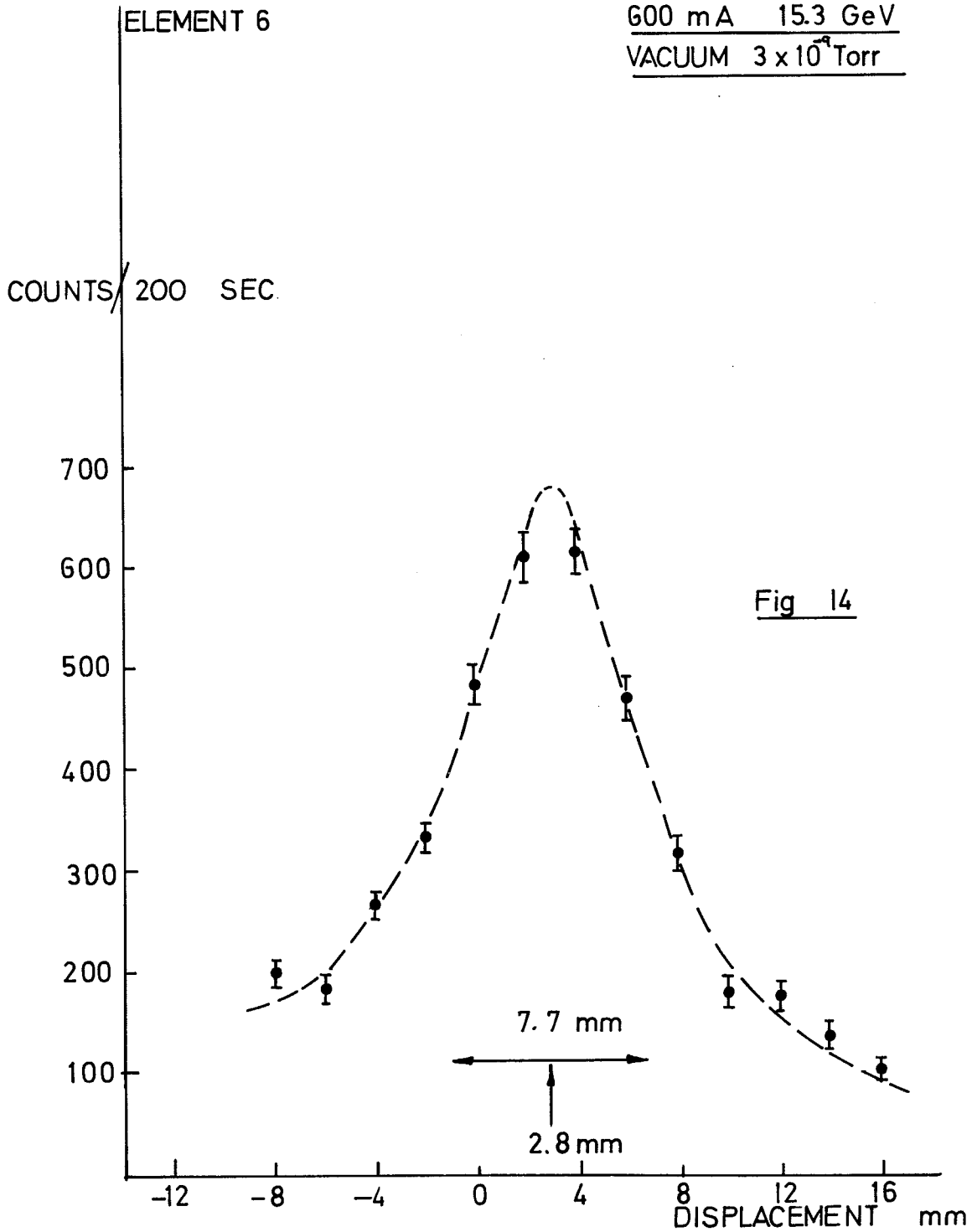

Fig 14

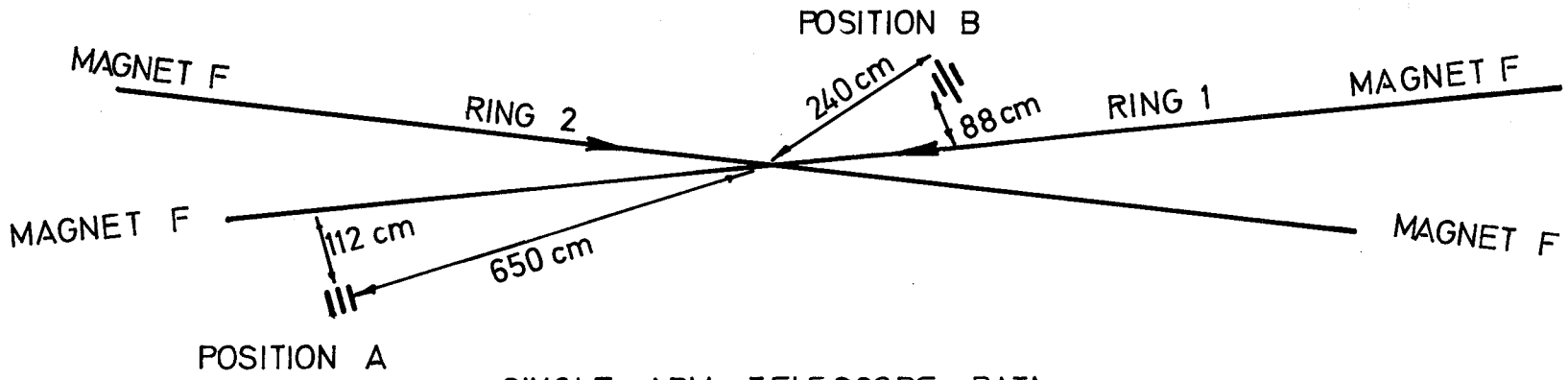

SINGLE ARM TELESCOPE DATA
AT LARGE ANGLES

Fig. 15

SINGLE ARM TELESCOPE DATA

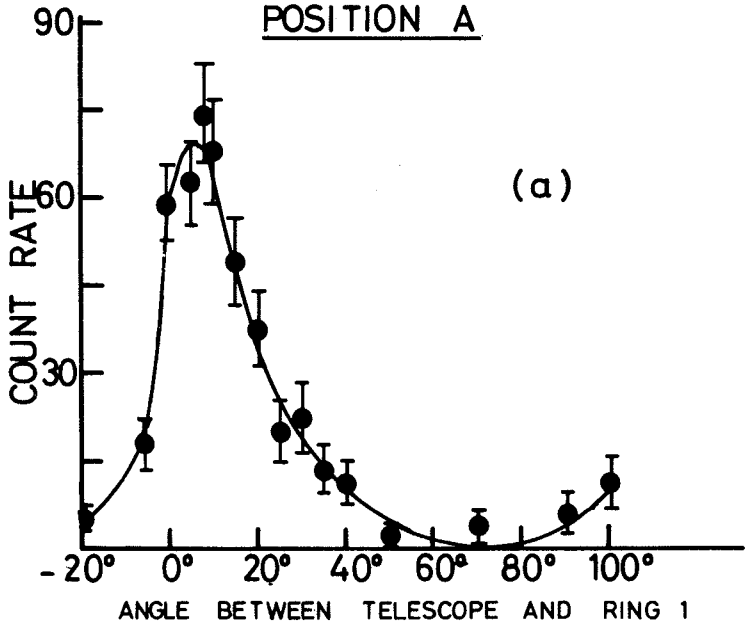

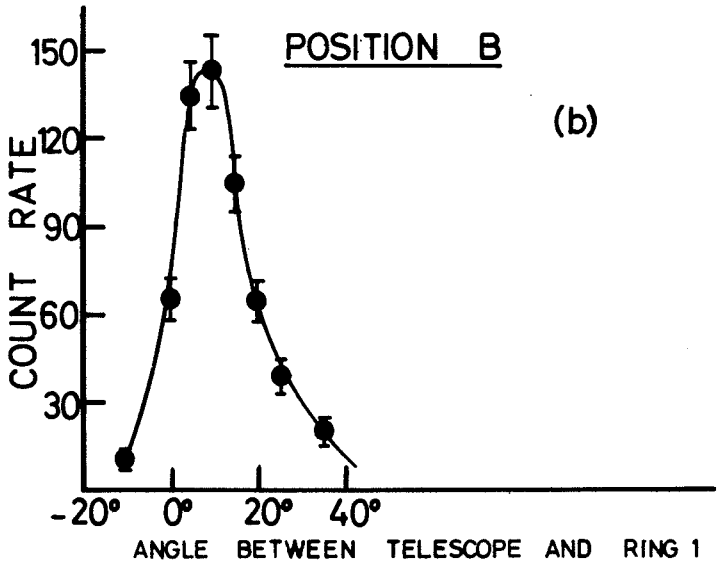

FIG 16

SINGLE ARM TELESCOPE DATA

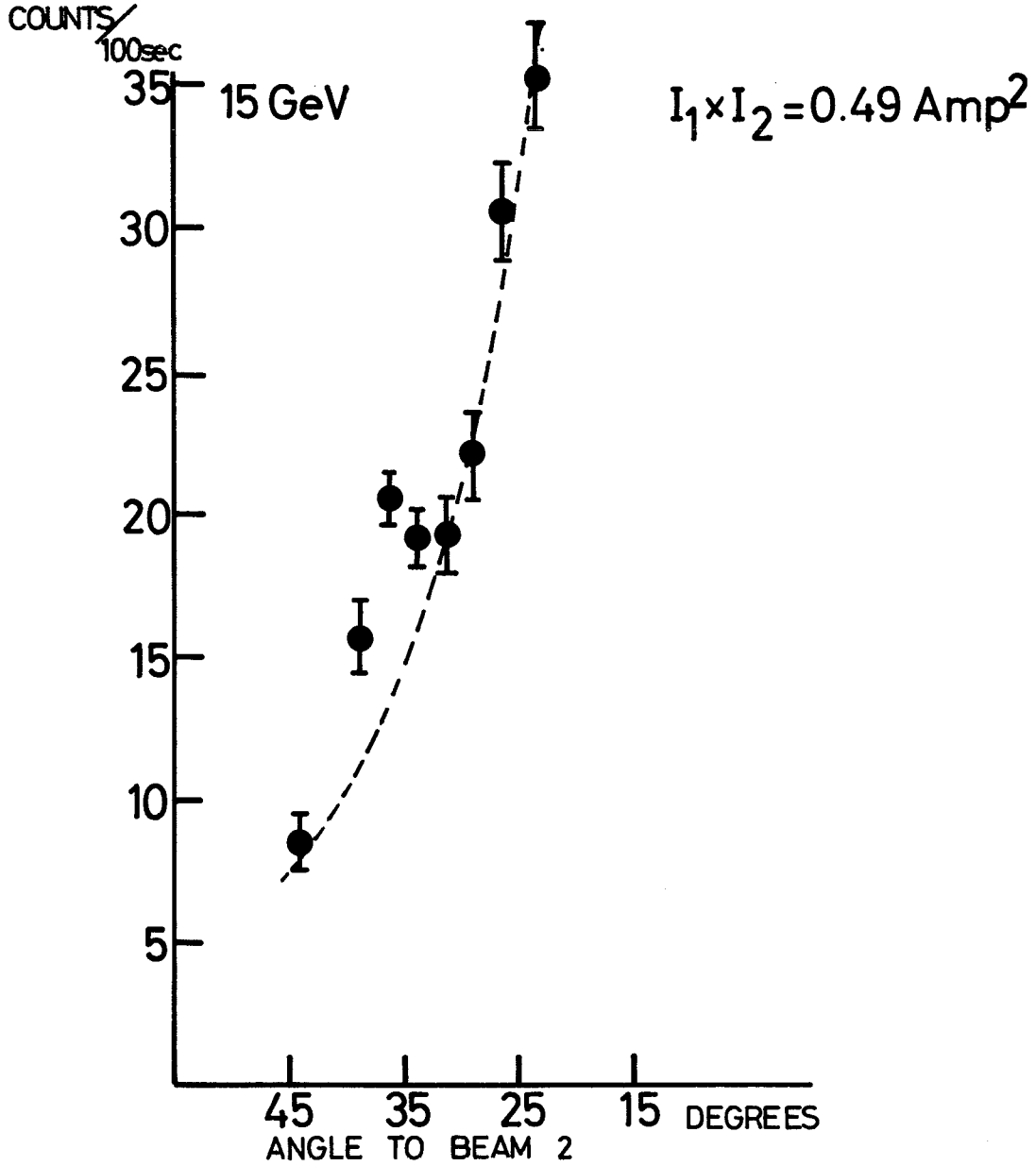

FIG. 17

SINGLE ARM TELESCOPE DATA

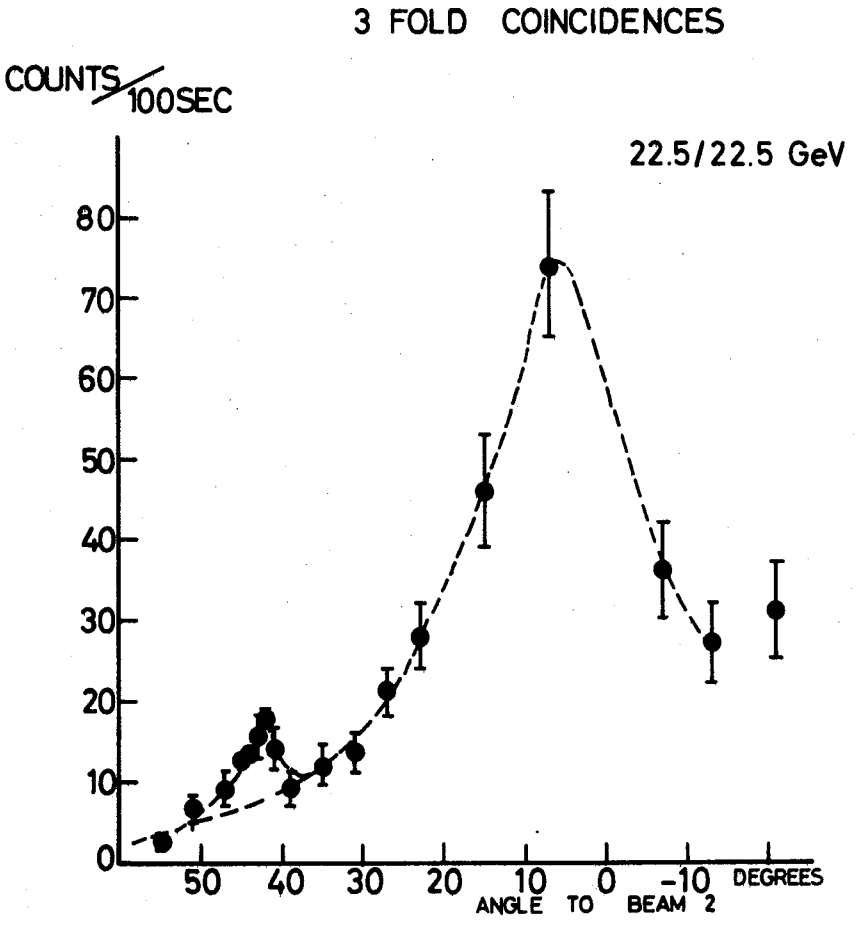

FIG 18

SINGLE ARM TELESCOPE DATA

4 FOLD COINCIDENCES

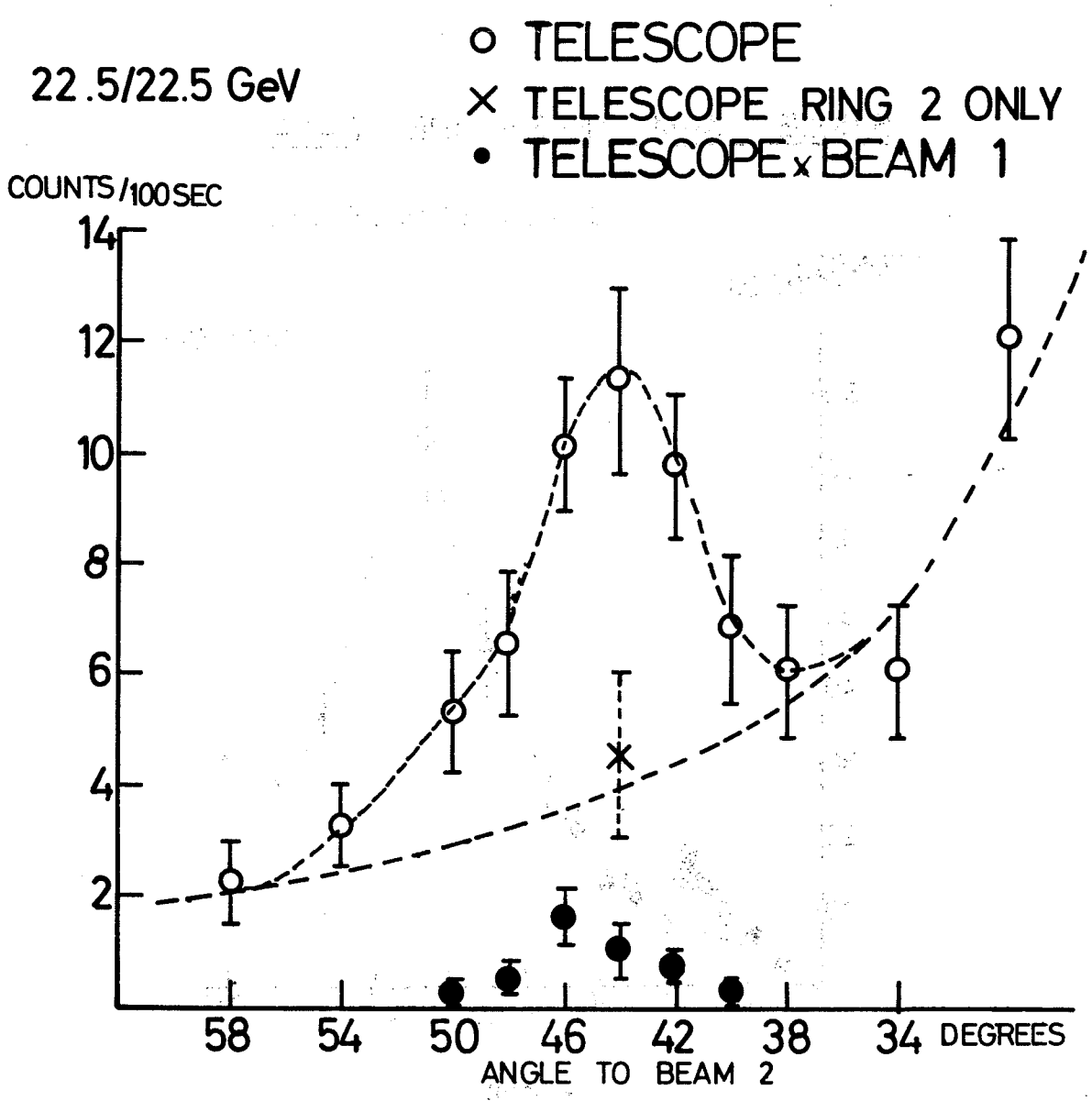

FIG. 19

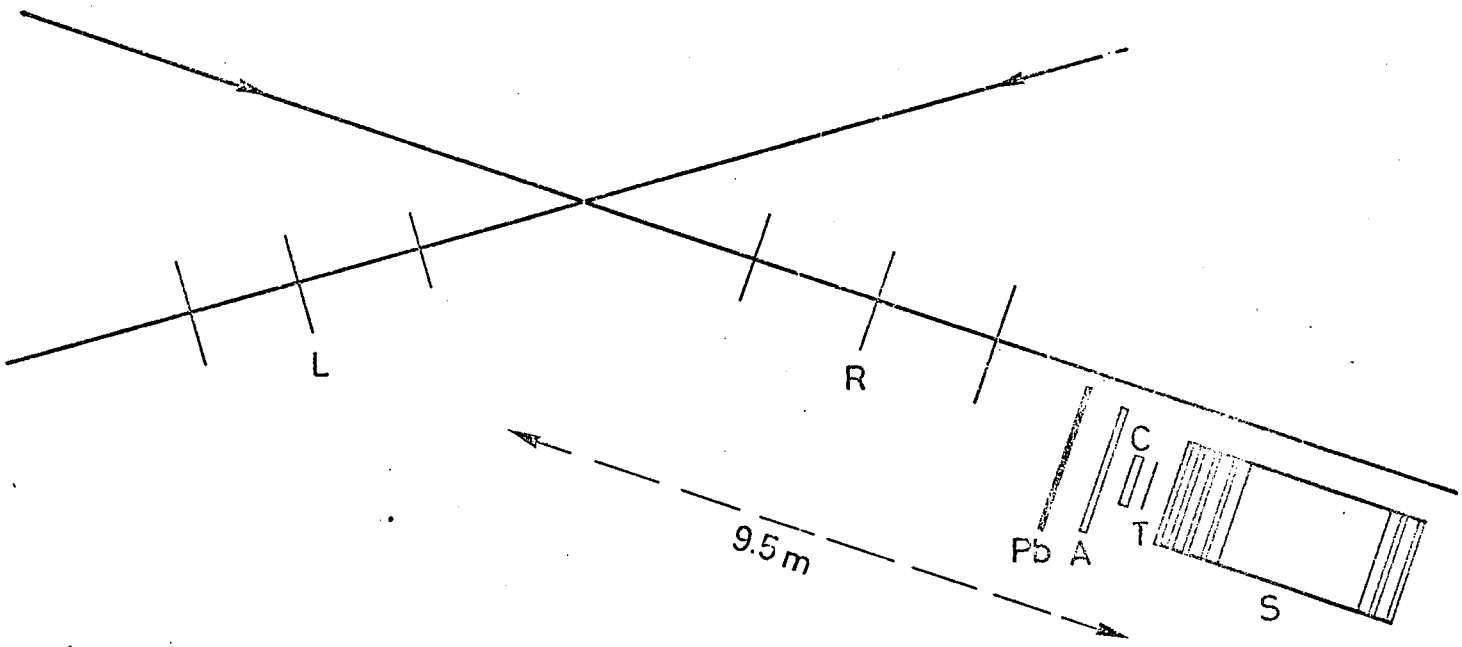

NEUTRON TOTAL ABSORPTION SPECTROMETER LAYOUT

FIG. 20

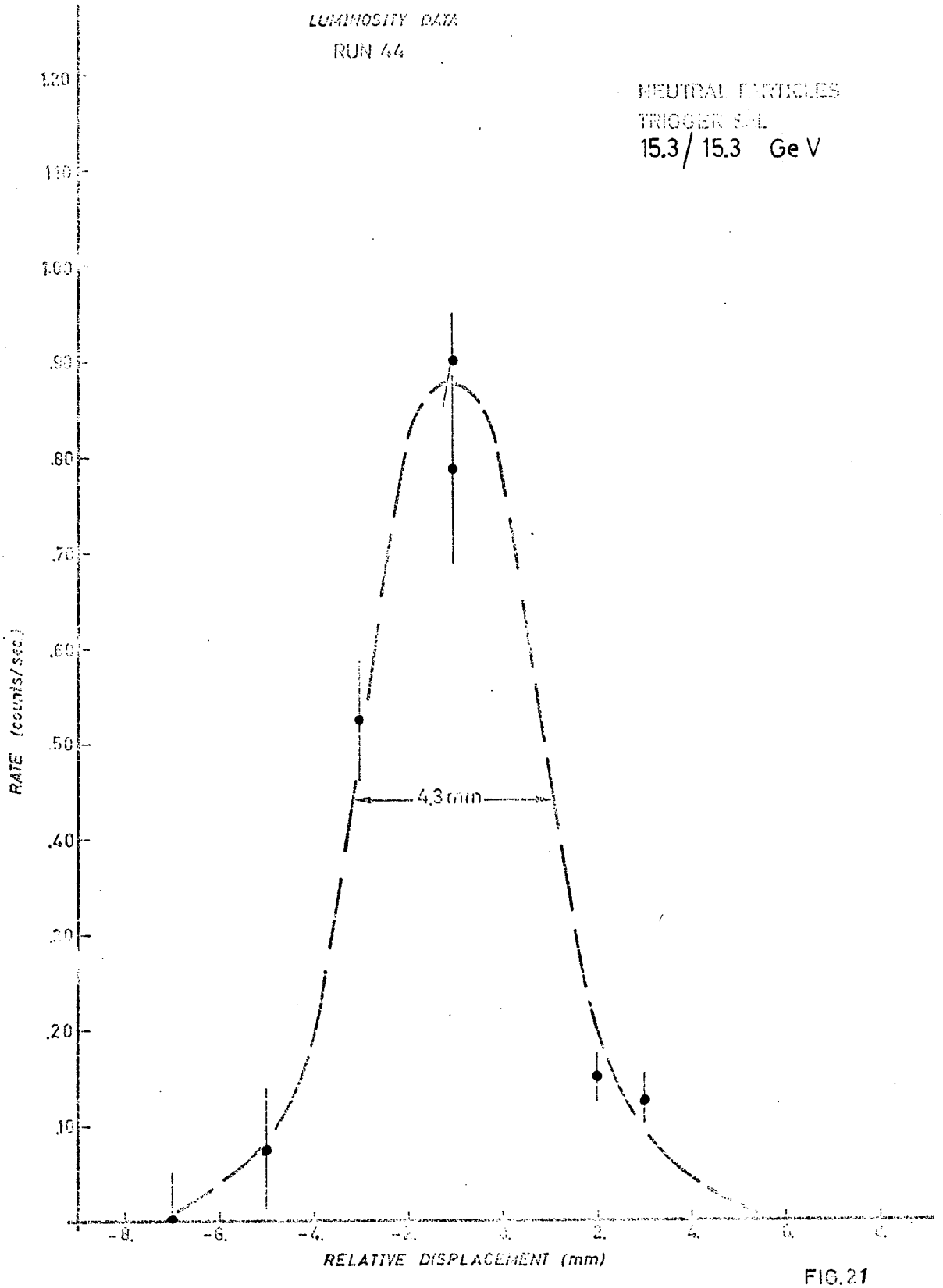
LUMINOSITY DATA
RUN 44
NEUTRAL PARTICLES
TRIGGER S-L
15.3 / 15.3 Ge V
1.20
1.00
.80
.70
.60
.50
.40
.20
.10
RATE (counts/sec)
4.3 mm
-8.
-6.
-4.
2.
4.
RELATIVE DISPLACEMENT (mm)

FIG. 21

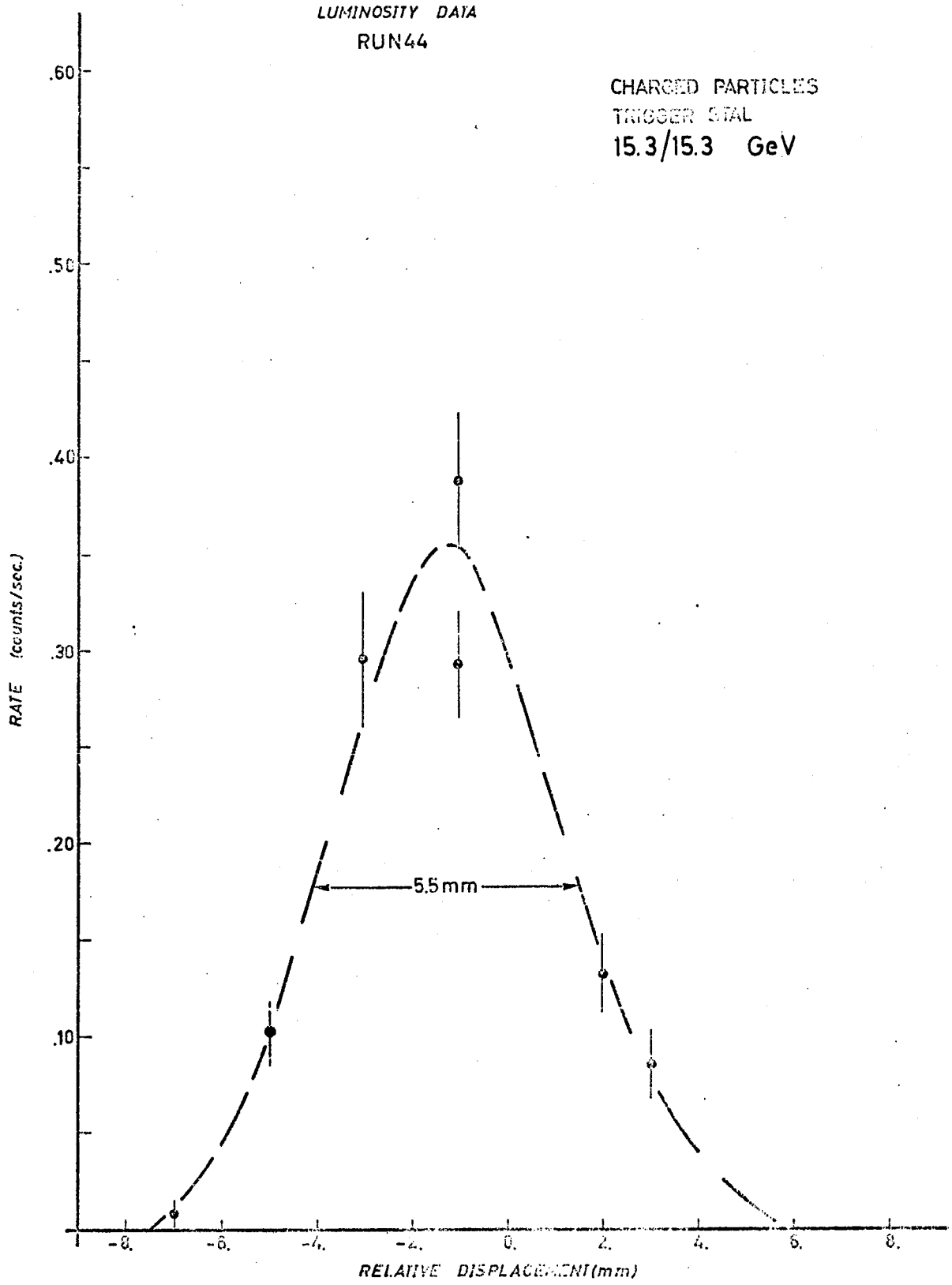
LUMINOSITY DATA
RUN44
CHARGED PARTICLES
TRIGGER STAL
15.3/15.3 GeV
.60
.50
.40
.30
.20
.10
RATE (counts/sec.)
5.5 mm
-8.
-6.
-4.
-2.
0.
2.
4.
6.
8.
RELATIVE DISPLACEMENT (mm)

FIG. 22

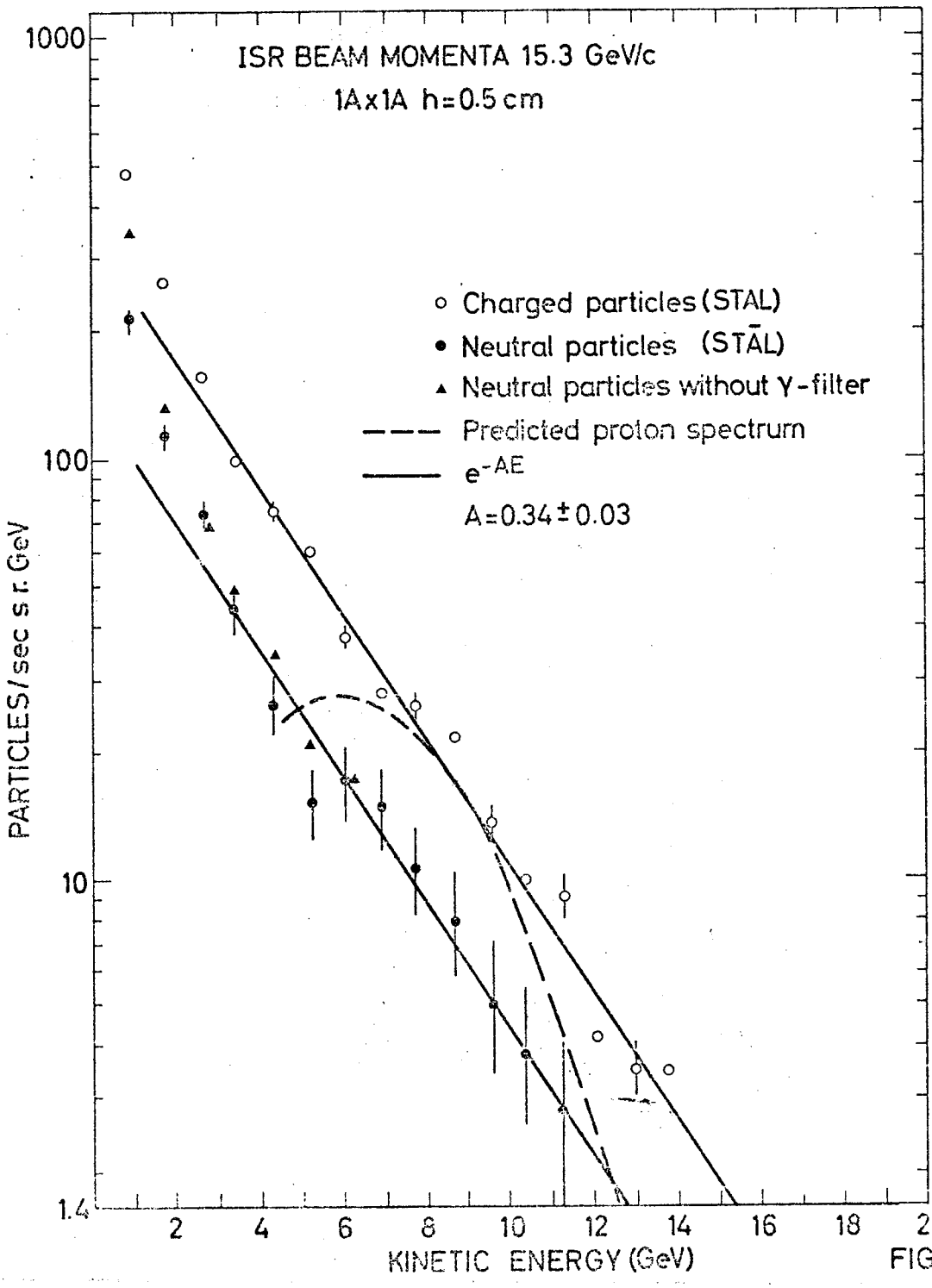
ISR BEAM MOMENTA 15.3 GeV/c
1Ax1A h=0.5 cm
Charged particles (STAL)
Neutral particles (STĀL)
Neutral particles without γ-filter
Predicted proton spectrum
e^-AE
A=0.34±0.03
PARTICLES/sec s r. GeV
KINETIC ENERGY (GeV)
1000
100
10
1.4
2
4
6
8
10
12
14
16
18
20

FIG 23

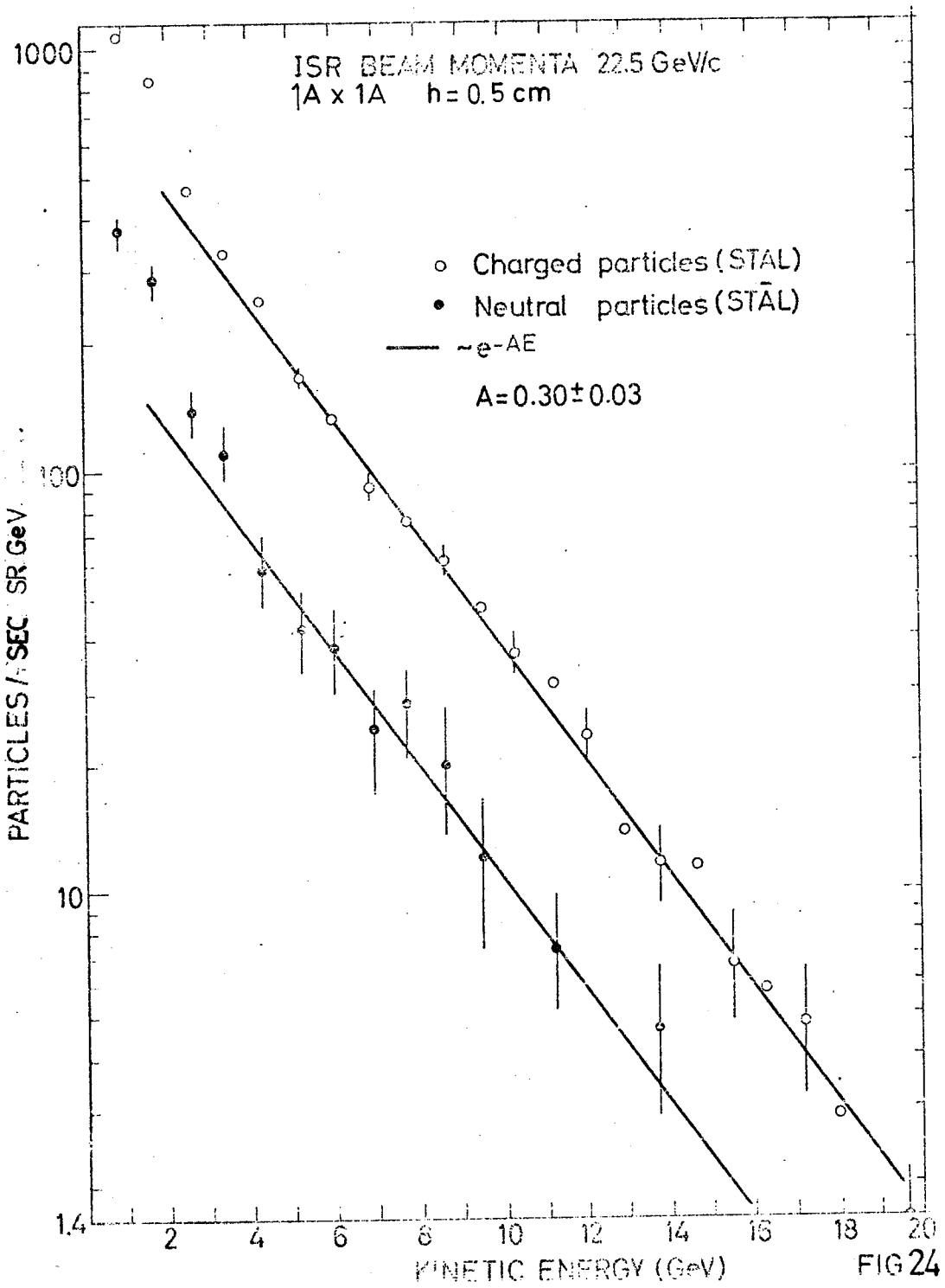
ISR BEAM MOMENTA 22.5 GeV/c
1A x 1A h = 0.5 cm
Charged particles (STAL)
Neutral particles (STAL)
~e-AE
A = 0.30 ± 0.03
PARTICLES / SEC SR GeV
1000
100
10
1.4
2
4
6
8
10
12
14
16
18
20
KINETIC ENERGY (GeV)

FIG 24

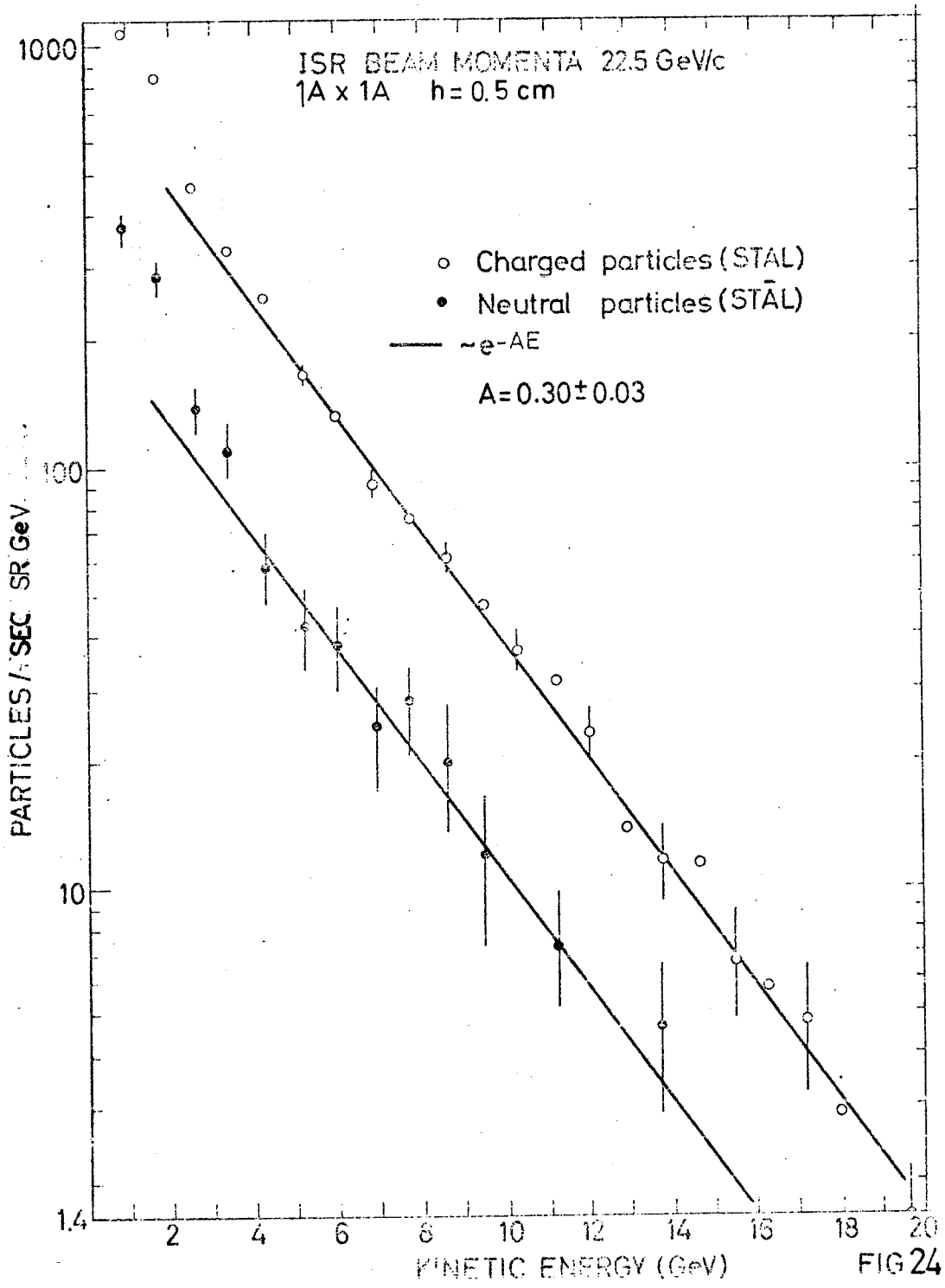
ISR BEAM MOMENTA 22.5 GeV/c
1A x 1A h = 0.5 cm
Charged particles (STAL)
Neutral particles (STĀL)
~e-AE
A = 0.30 ± 0.03
PARTICLES / SEC SR GeV
1000
100
10
1.4
2
4
6
8
10
12
14
16
18
20
KINETIC ENERGY (GeV)

FIG 24

GAMMA-RAY DETECTOR LAYOUT

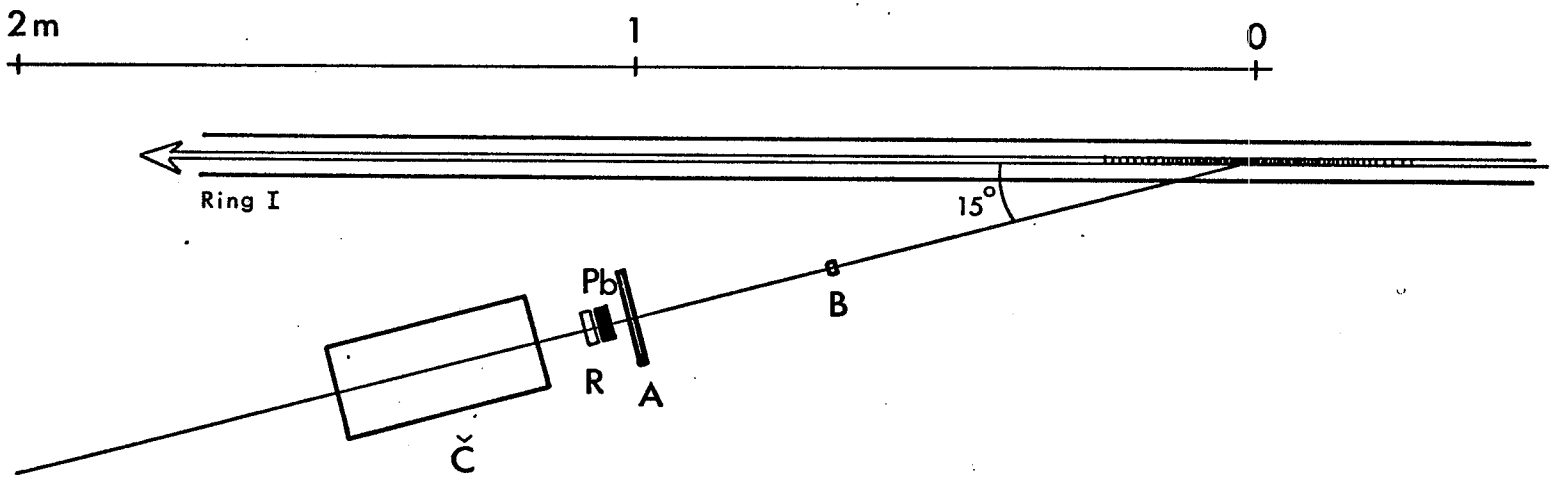

B 2 cm ∅
R 5×5 cm^2
Pb 5.8 mm thick
A 15 cm ∅
Č 32 cm × 13.8 cm ∅

CHOV

Fig. 25

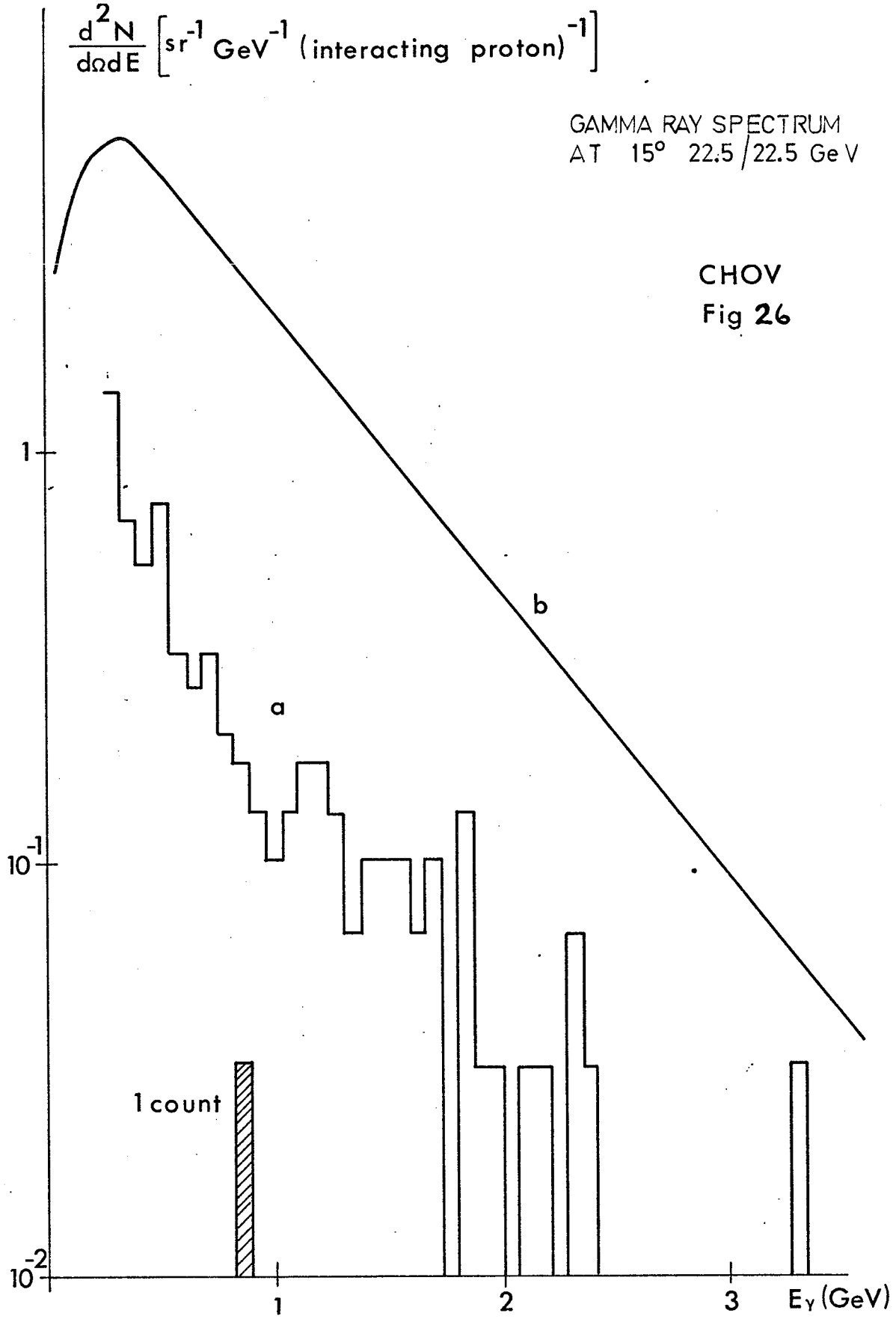
$\frac{d^2N}{d\Omega dE}$ [sr^{-1} GeV^{-1} (interacting proton)$^{-1}$]
GAMMA RAY SPECTRUM
AT 15° 22.5/22.5 GeV
CHOV
Fig 26
1
10^{-1}
10^{-2}
a
b
1 count
1
2
3
E_γ (GeV)

90° TELESCOPE LAYOUT

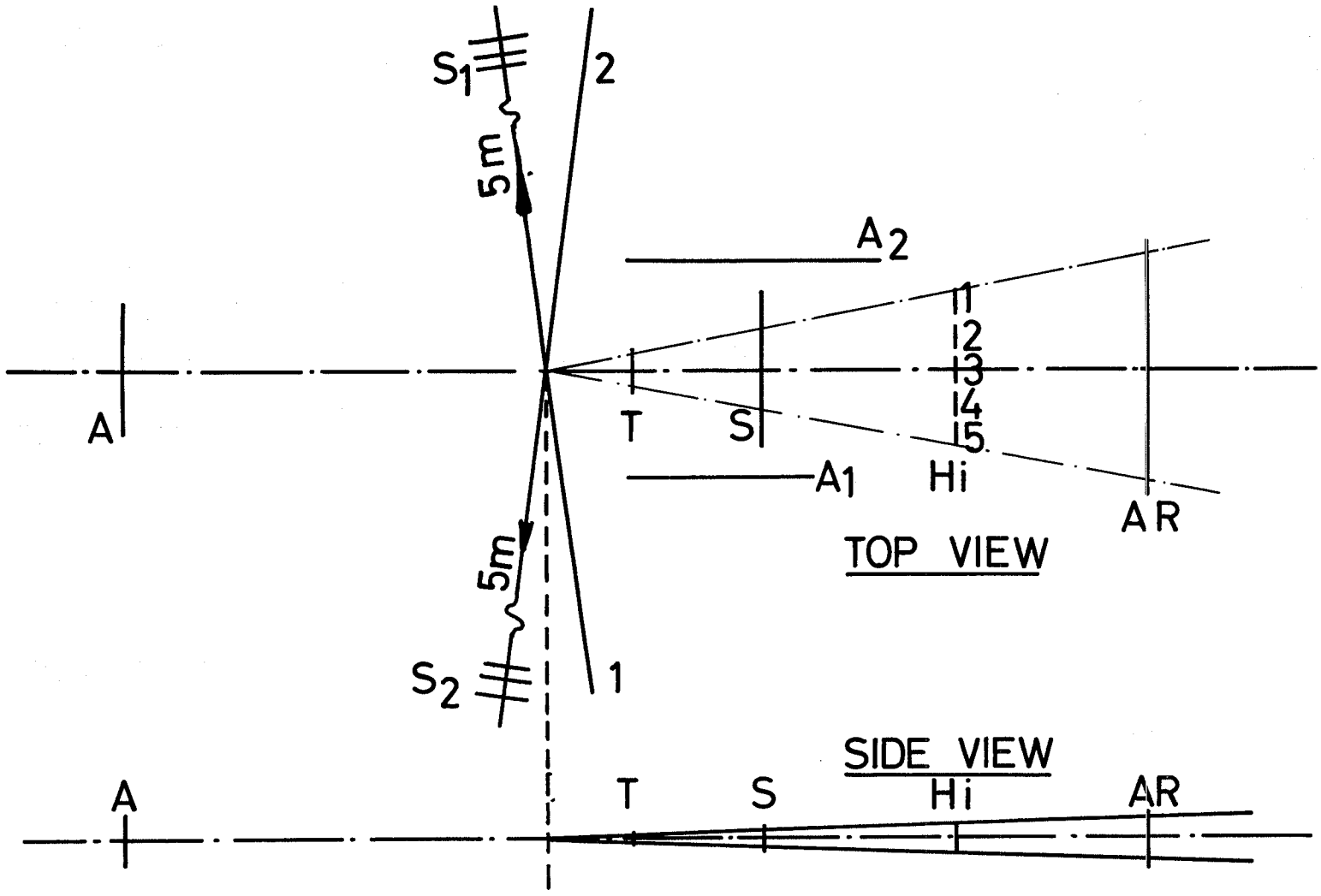

SCALE : 1/20

FIG. 27

90° TELESCOPE DATA

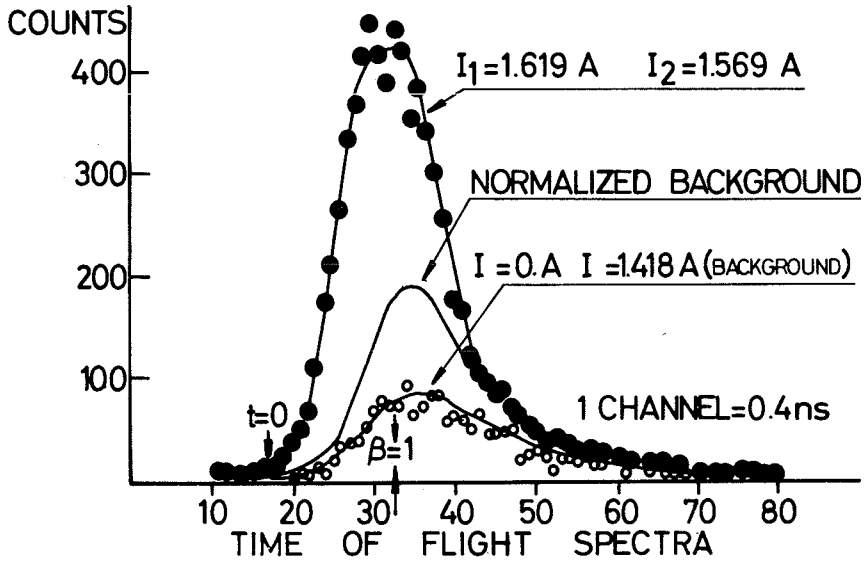

FIG 28

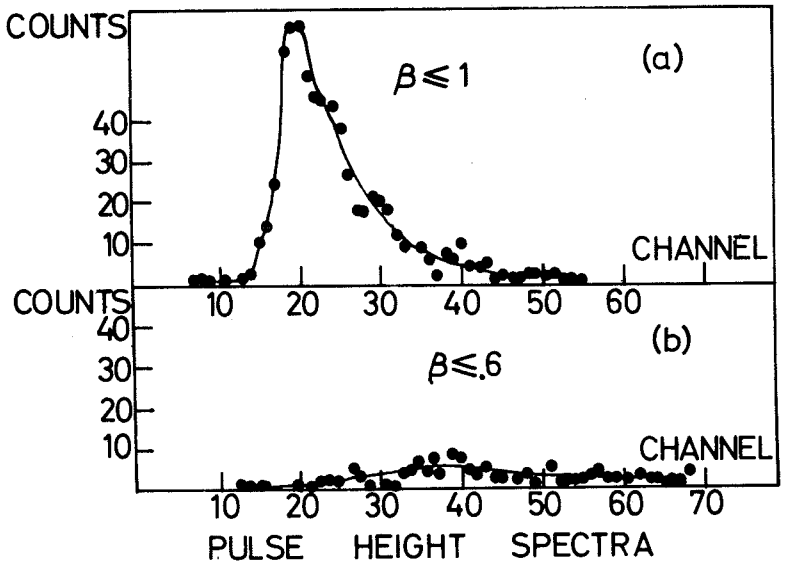

FIG 29

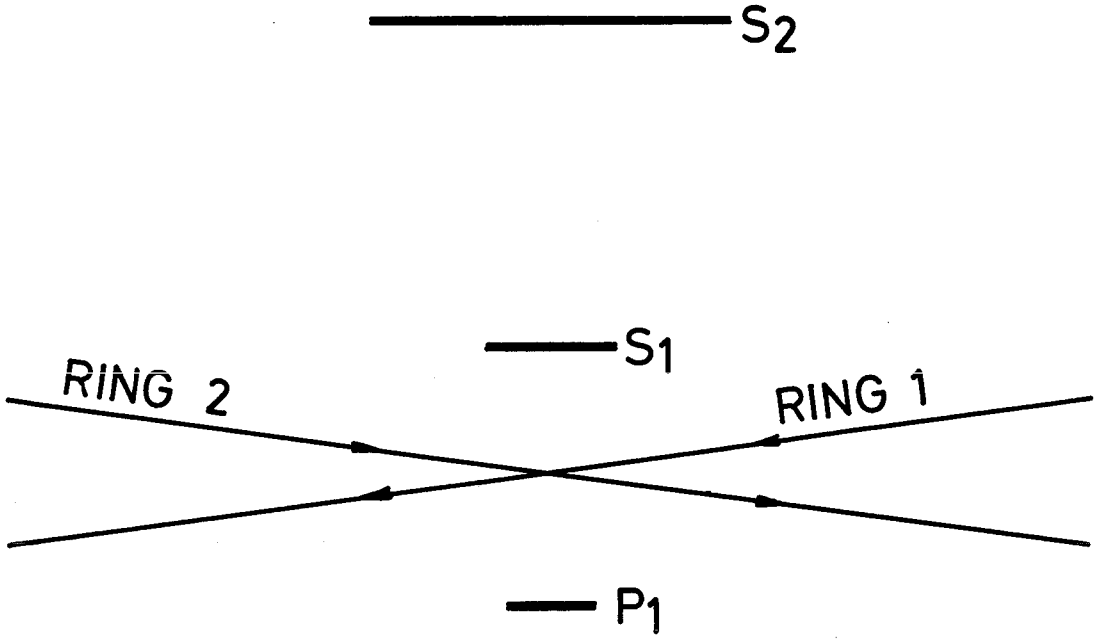

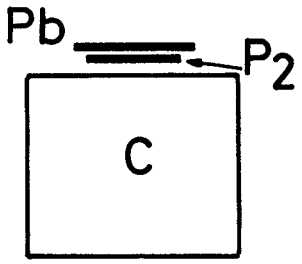

LEAD GLASS COUNTER ARRANGEMENT AT 90°

TOP VIEW

FIG. 30

50 cm

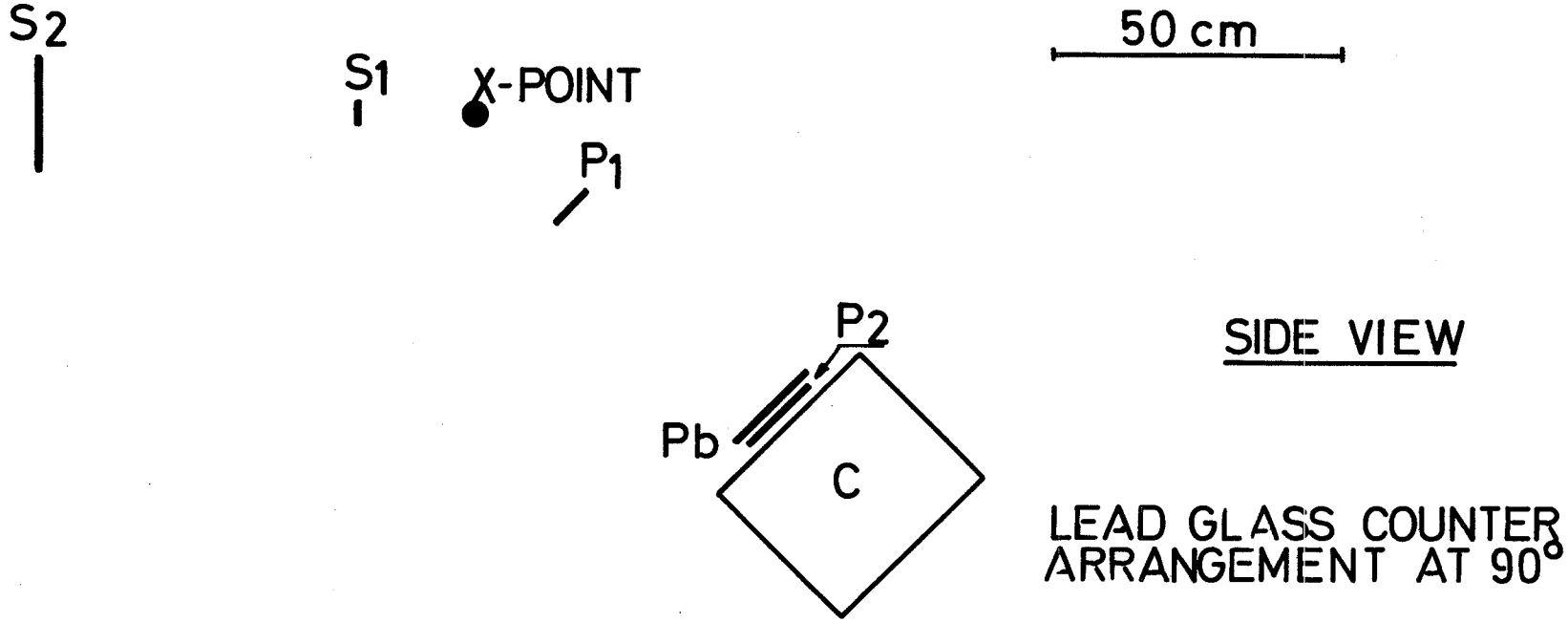
S2
S1
X-POINT
P1
50 cm
P2
Pb
C
SIDE VIEW
LEAD GLASS COUNTER
ARRANGEMENT AT 90°
P3

FIG. 31

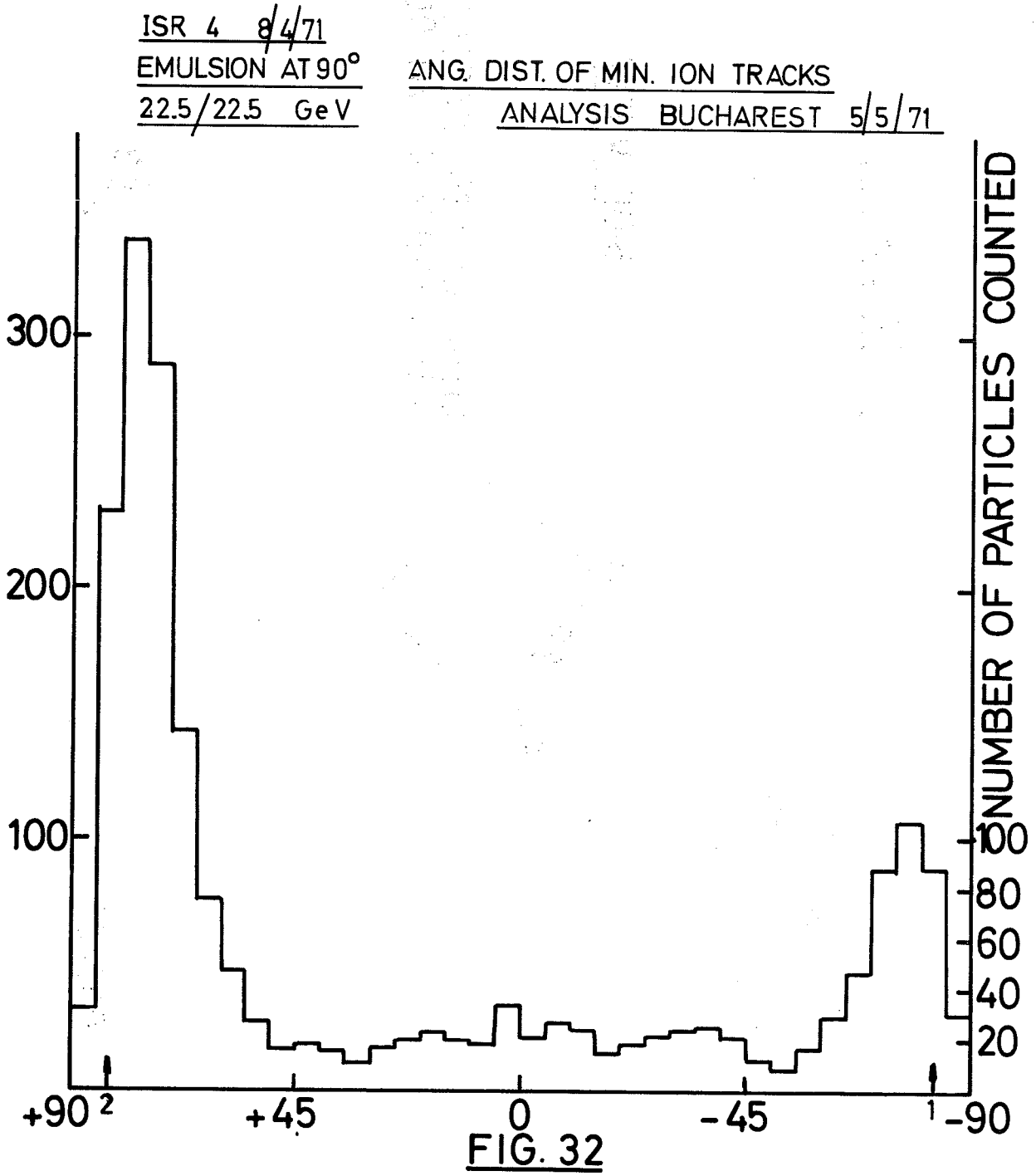
ISR 4 8/4/71
EMULSION AT 90°
22.5/22.5 GeV
ANG. DIST. OF MIN. ION TRACKS
ANALYSIS BUCHAREST 5/5/71
NUMBER OF PARTICLES COUNTED
300
200
100
100
80
60
40
20
+90
+45
0
-45
-90
2
1

FIG. 32

ISR 2 30/3/71
EMULSION AT 90°
15.3/15.3 GeV

ANG. DIST. OF MIN. ION TRACKS
ANALYSIS BUCHAREST 5/5/71

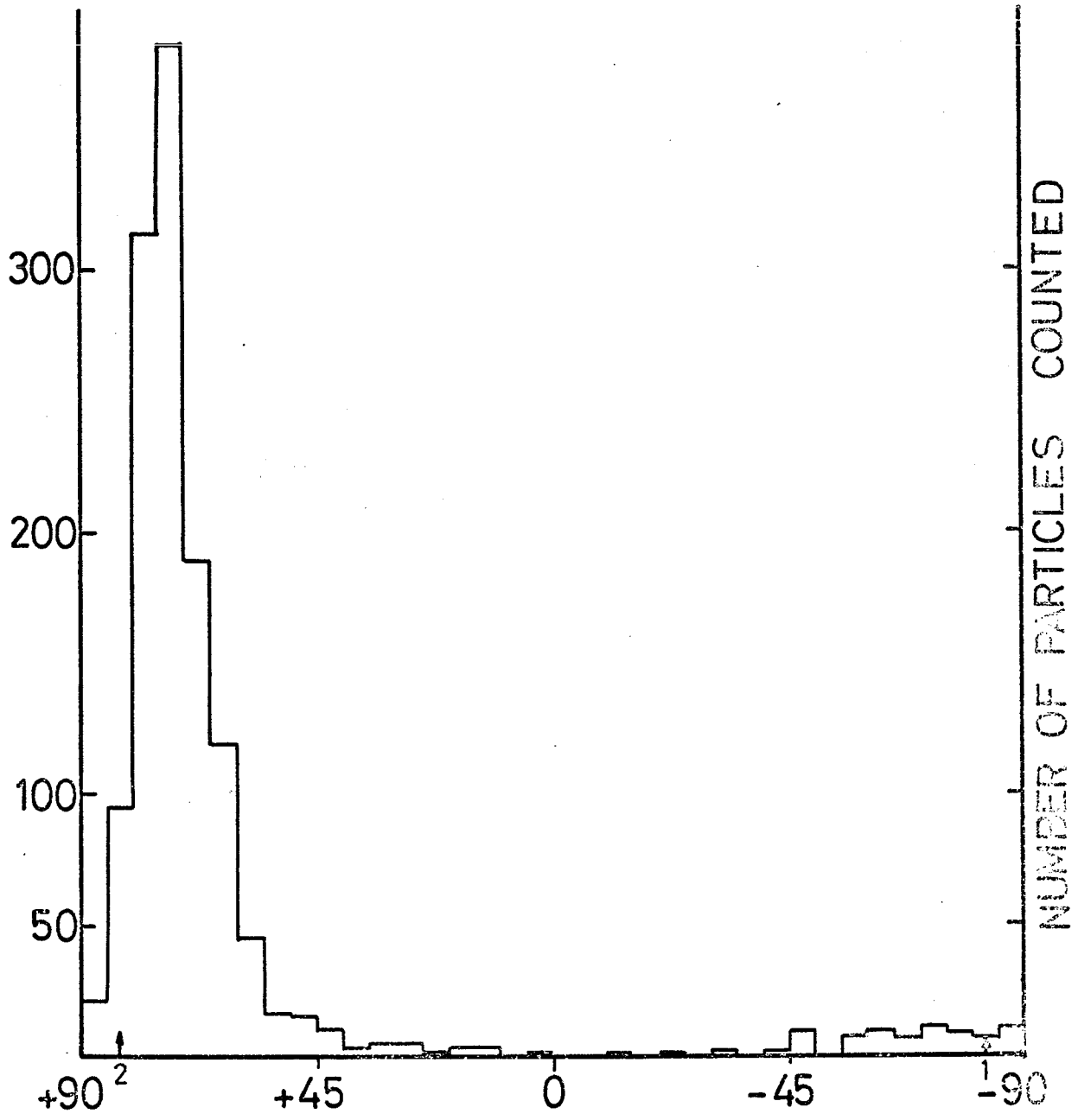

FIG. 33

EMULSION DATA 5/5/71

DIFFERENCE BETWEEN ISR 4 & ISR 2

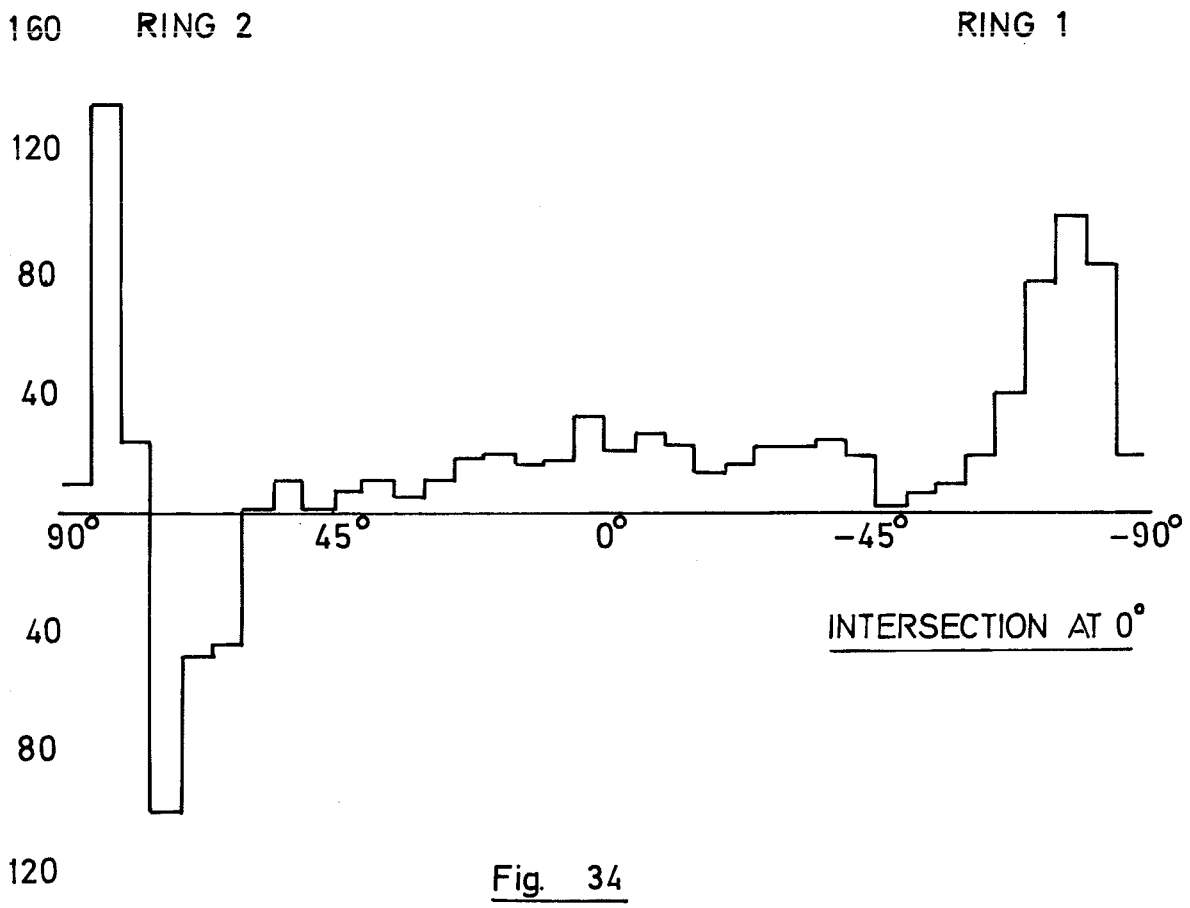

Fig. 34

γ RAY ANGULAR DISTRIBUTION
IN PLATE 2 (K5S) ISR4 8/4/71

EMULSION DATA 15.3/15.3 GeV

Fig 35

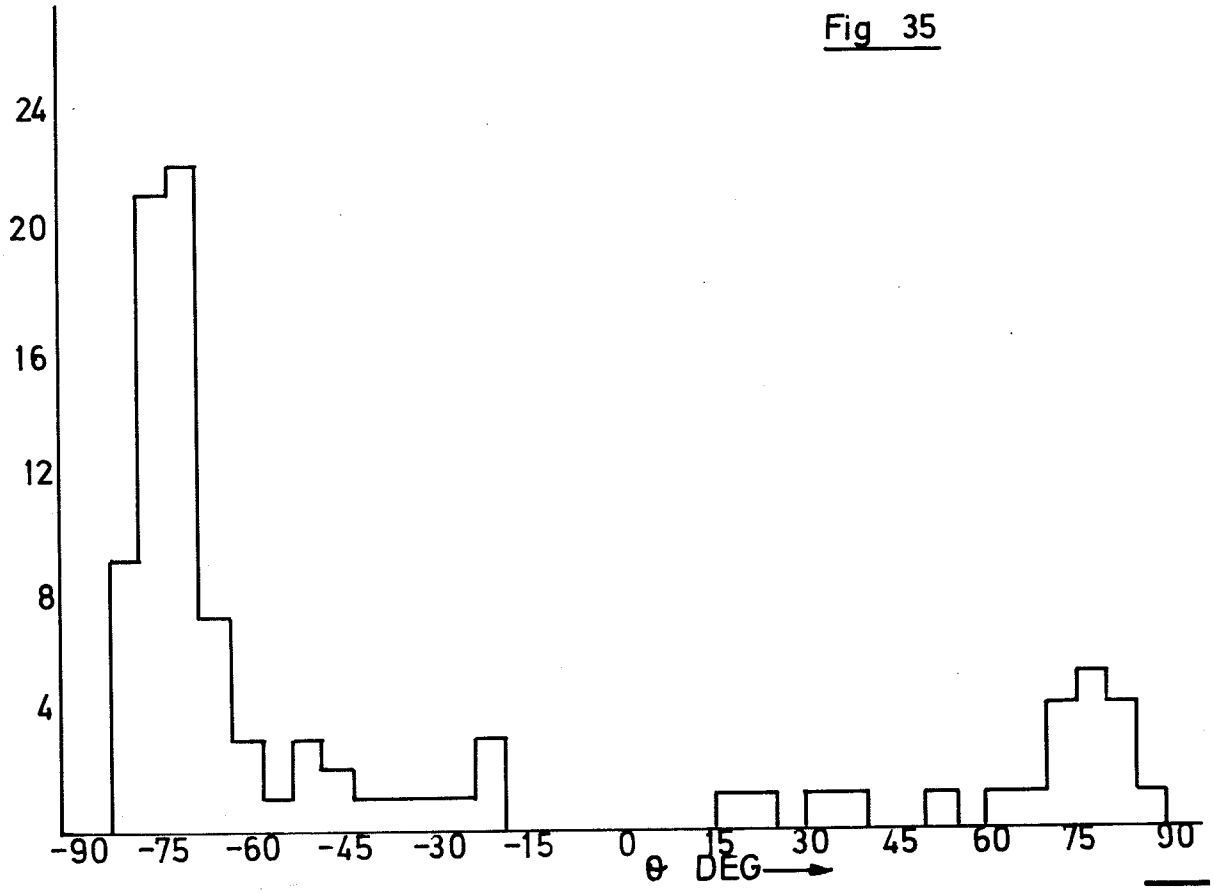

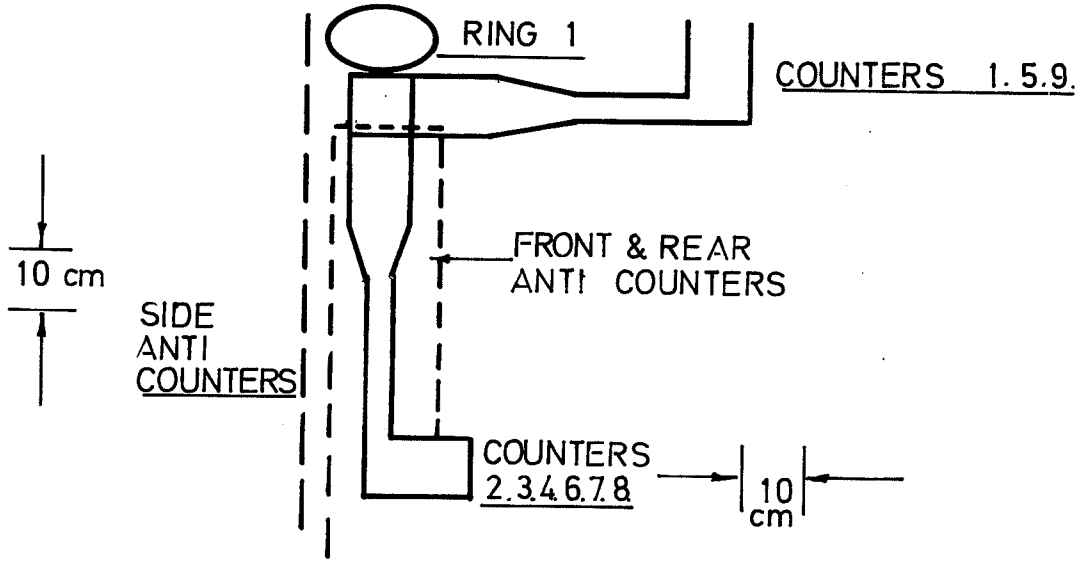
RING 1
COUNTERS 1.5.9.
10 cm
SIDE
ANTI
COUNTERS
FRONT & REAR
ANTI COUNTERS
COUNTERS
2.3.4.6.7.8
10
cm

Fig 36

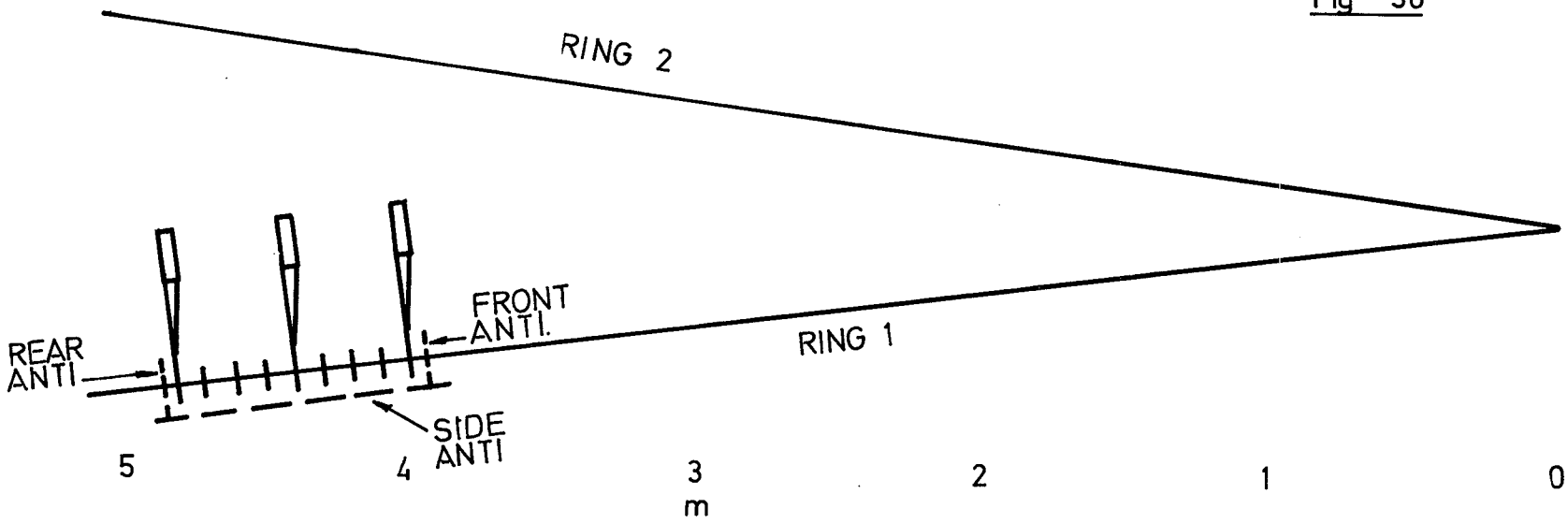
RING 2
FRONT
ANTI.
REAR
ANTI
RING 1
SIDE
ANTI
5
4
3
2
1
0
m

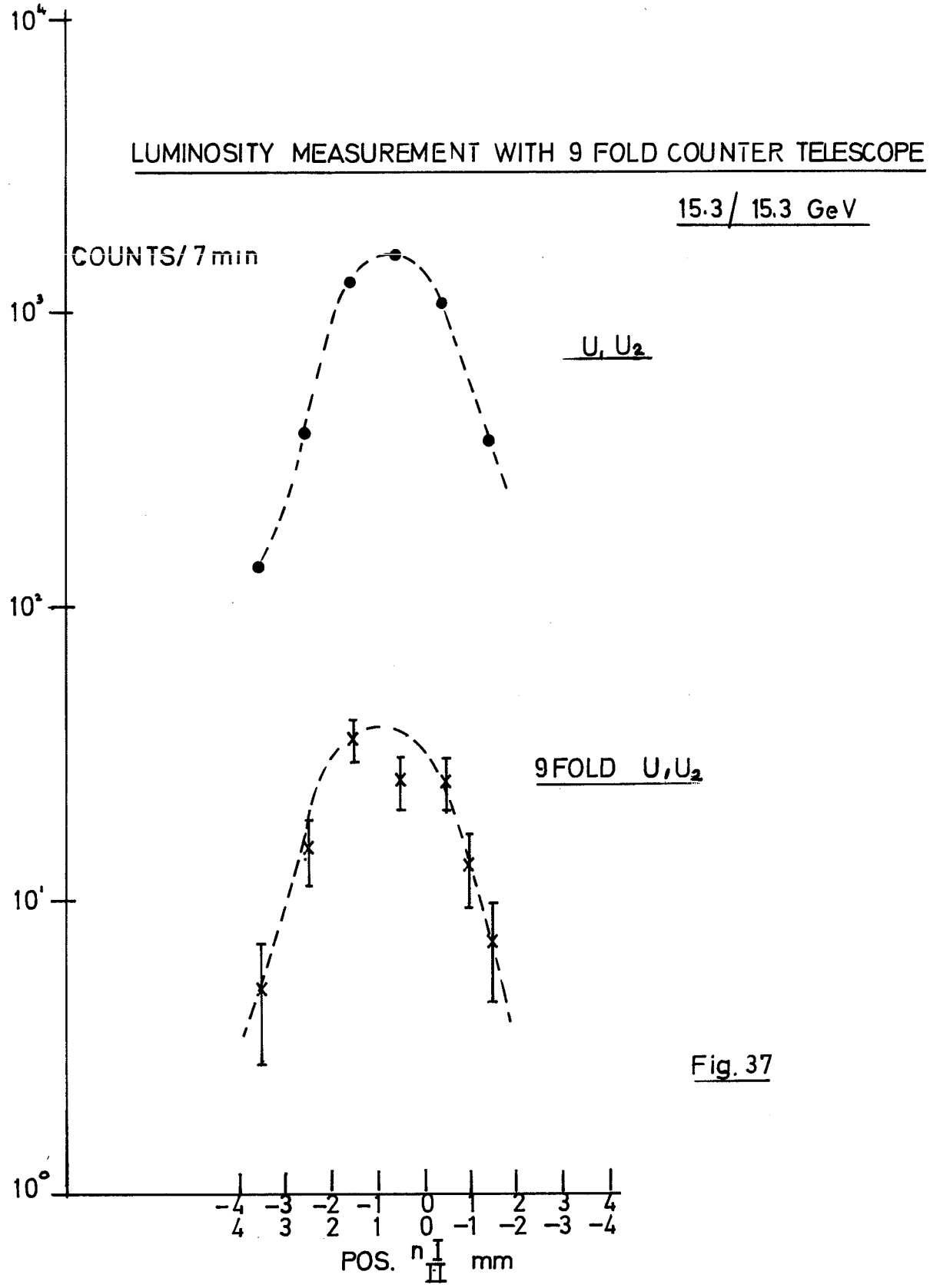
LUMINOSITY MEASUREMENT WITH 9 FOLD COUNTER TELESCOPE
15.3 / 15.3 GeV
COUNTS/ 7 min
10^4
10^3
10^2
10^1
10^0
U, U_2
9 FOLD U, U_2
-4 -3 -2 -1 0 1 2 3 4
4 3 2 1 0 -1 -2 -3 -4
POS. $n\frac{I}{II}$ mm

Fig. 37

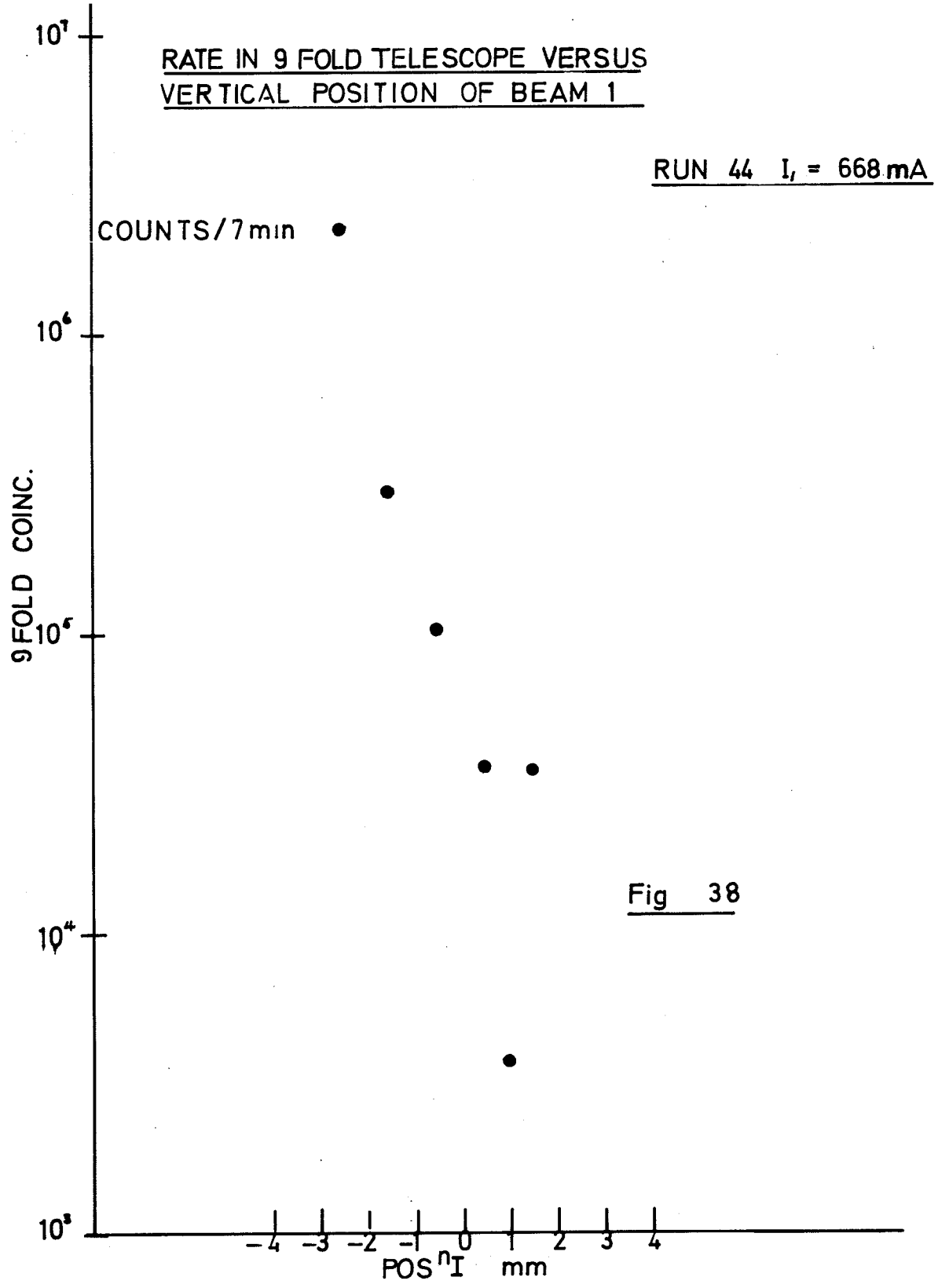
RATE IN 9 FOLD TELESCOPE VERSUS
VERTICAL POSITION OF BEAM 1
RUN 44 I_1 = 668 mA
COUNTS/7 min
9 FOLD COINC.
10^7
10^6
10^5
10^4
10^3
−4 −3 −2 −1 0 1 2 3 4
POS ^{n}I mm

Fig 38